Journal of Inorganic and Organometallic Polymers and Materials (2021) 31:4103–4125
https://doi.org/10.1007/s10904-021-02029-7

Radiation Synthesis and Characterization of Poly (vinyl alcohol)/acrylamide/TiO_2/SiO_2 Nanocomposite for Removal of Metal Ion and Dye from Wastewater

Ahmed M. Elbarbary[1] · **Yasser H. Gad**[1]

Received: 18 March 2021 / Accepted: 17 May 2021 / Published online: 25 May 2021

Abstract

PVA-co-AAm/TiO_2/SiO_2 nanocomposites adsorbents synthesized by γ-irradiation copolymerization of polyvinyl alcohol (PVA) and acrylamide (AAm) incorporated TiO_2/SiO_2 nanopowders, aiming to enhance the removal of basic blue 3 dye (BB3) and Cu (II) ions from aqueous solutions. Properties of nanocomposites were analyzed by different techniques. FTIR results showed successful incorporation of nanoparticles and copolymerization of PVA and AAM. SEM/EDS confirm the peaks belonging to C, O, Si, and Ti. TEM investigation illustrated that TiO_2/SiO_2 nanoparticles were well dispersion, uniform, and homogeneous shape of particle size of 60–70 nm. XRD data specified characteristic diffraction peaks of TiO_2 and the calculated crystalline size was 43 nm. Adsorption results confirm that PVA-co-AAm/TiO_2/SiO_2 nanocomposites provide better adsorption capacities of both BB3 and Cu (II) was three-folds rather than PVA-co-AAm-30. The nanocomposite prepared at 30 kGy (PVA-co-AAm/TiO_2/SiO_2-30) showed high swelling, gelation, and highest adsorption capacity and it was selected as the best adsorbent for batch experiments. The optimum adsorption was achieved using 0.4 g PVA-co-AAm/TiO_2/SiO_2-30 adsorbent dosage. The adsorption capacity of BB3 and Cu (II) was 140.9 and 190.3 mg/g with a removal efficiency of 93.5 and 95.2% after 7 h and 6 h, pH 11 and pH 6, and initial concentration of 150 and 200 mg/L, respectively. The adsorption of BB3 or Cu (II) was endothermic and spontaneous, well described by the pseudo-second-order adsorption kinetic and fit Langmuir isotherm. The results revealed that the as-synthesized PVA-co-AAm/TiO_2/SiO_2 nanocomposites could be employed as effective adsorbents for the adsorption of BB3 and Cu (II) ions from wastewater with high adsorption capacity and recovery.

Keywords Radiation polymerization · PVA, · Acrylamide · TiO_2 · SiO2, · Nanocomposite · Basic blue 3 dye · Copper ions · Adsorption · Removal

1 Introduction

Heavy metals ions like Cu (II) ions and organic dyes like basic blue 3, acid violet 7 crystal, methylene blue, methyl orange, and others are considered as striking chemicals in various industries wastewater effluents. These pollutants lead to environmental risks as a group of harmful carcinogens [1]. One of the difficulties correlated with the occurrence of dyes and heavy metals in wastewater is that they are not biodegradable in aquatic media and highly soluble pollutants therefore they can be consumed by organisms, and consequently, go into the food chain. Although the human body contains copper and plays a significant function in the development of bones and tissues or enzyme creation [2]. On the other hand, an overload of Cu (II) ions and its deposition in the body is poisonous and causes a severe impact like headache, gastrointestinal bleeding, kidney and liver failure, and cancer [3]. Thus, the elimination of Cu (II) ions from water and wastewater is crucially significant for the protection of the health and environment. The elimination of pollutants like dyes, metals, and pigments from wastewater is significant for water pollution [4].

✉ Ahmed M. Elbarbary
amelbarbary@yahoo.com; ahmed.elbarbary.mansour@gmail.com; ahmed.elbarbary@eaea.org.eg

[1] Radiation Research of Polymer Chemistry Department, National Center for Radiation Research and Technology, Egyptian Atomic Energy Authority, Cairo, Egypt

A variety of procedures have been created for the elimination of toxic pollutants from wastewater like ion exchange, flotation membrane filtration, electrochemical treatment, photocatalysis, chemical precipitation, and adsorption [5]. The adsorption process is an effective, simple, and useful method for pollutant elimination. Using a suitable adsorbent makes the adsorption process suitable, low cost, ease of operation, versatility, and an effective method for the elimination of dyes and metals from wastewater.

Nanotechnologies provide a wide range of applications like water treatment, soil treatment, environmental remediation, sustainable agriculture, and the production of renewable energy. Nanomaterials have several advantages over bulk materials such as the large surface area, the huge surface-to-volume ratio, improved reactivity, high porosity, and completely different physiochemical properties. Nowadays, nanomaterials or nanostructures are considered novel categories of functional substances with distinctive properties and efficient applications in various fields [6]. Nanocomposites are a major class of nanomaterials and have been widely used as an adsorbent in environmental remediation for metal ions or dye removal with high adsorption capacity due to their suitable pore size, high mechanical strength, ease production, high selectivity, and regeneration processes [7]. Therefore, the nanostructures as effective materials for several applications such as electrochemical hydrogen storage [8, 9], removal and degradation of organic pollutants and contaminants [10–12], surface decontamination in fuel manufacture plants [13], anion exchange resin [14], energy storage and conversion [15], biomolecular imaging and therapy [16], animals biodistribution studies [17, 18] and biomedical applications with the ultimate goal of efficiently diagnosing and treating various human diseases [19], etc.

Recently, polymer-based nanocomposites consist of polymer or copolymer having nanoparticles dispersed in their polymer matrix and incorporate the remarkable features of both NPs and polymers developed owing to their advantages properties the unique physicochemical properties such as film-forming ability with variable dimensions and their high functionalities [20] resulting from the large surface area to volume ratios, the high interfacial reactivity of nanoparticles, the compatibility. These features made polymer-based nanocomposites of a promising class of adsorbent materials for dyes and metals removal from water and wastewater [21]. Many polymer-based nanocomposites have widely utilized for the elimination of a variety of toxic dyes and metal ions, from water and wastewater for example magnetic chitosan/Al_2O_3/Fe_3O_4 nanocomposite for removing acid fuchsin dye [22], titanate layer–natural polymer amylopectin based nanocomposite for adsorption and separation of methylene blue and methyl orange dyes [23], carboxymethyl-chitosan /bentonite composite for adsorption of Cu^{2+} ions [24], polyaniline/carboxymethyl cellulose/TiO_2 nanocomposites for adsorption of congo red dye [25], TiO_2-chitosan-polyacrylamide for the uptake of Sirius yellow K-CF dye [26], TiO_2-Kaolinite nanocomposite for adsorption of Pb (II) and Cd(II) ions [27].

Several methods are used for the preparation of nanocomposite by incorporation of nanomaterials into a polymer through physical blending (mixing), crosslinking and polymerization reactions with monomers, solution casting method, and hot press [28]. Gamma radiation is one of the suitable methods for the preparation of polymer-metal nanocomposite by mixing the metal salt and organic monomer solution. During gamma irradiation and polymerization reaction, a homogeneous dispersion of nanocrystalline metal particles and polymerization of monomer created instantaneously. Many nanocomposites are prepared by gamma radiation for different applications including different metal nanoparticles [17, 29–31]. Radiation is a convenient tool for the cross-linking and modification of polymeric materials without using a cross-linking reagent. This technology is environmentally friendly since it leaves no residue or pollutant in the environment [32, 33].

PVA is a synthetic polymer soluble in water used in various industrial, pharmaceutical, medical, environmental, and agricultural applications as a result of its low cost, chemical and physical resistance, and amazing film-forming property [34]. Acrylamide (AAm) or acrylamide-based polymers is one of the water-soluble polymers that carry a negative charge and are used for a variety of applications in lubrication, effluent reclaiming, mining, Paper manufacture, and water management process [35].

One of the most important metal oxides is titanium dioxide (TiO_2) as catalytic and material used for the removal and adsorption of metals or dyes. TiO_2 has been widely used owing to its low economic cost and high efficiency in pollution degradation. TiO_2 can be used in many industrial applications like environmental purification for the removal of various pollutants due to their photocatalytic properties [36], photovoltaic devices, solar energy conversion, and optical coating photocatalysis [37]. It is important to improve the efficiency of TiO_2 for use in catalytic applications, through the combination of the photoactive TiO_2 material with another metal oxide such as SiO_2. Nanomaterials of TiO_2 and SiO_2, offer greater surface area than their bulk counterparts, allowing for improved application performance. The coating of the surface of TiO_2 nanoparticles with SiO_2 promotes their adsorption property, prevents their aggregation, and improves their thermal and chemical stability. An improved photocatalyst of a mixed oxide of TiO_2 and SiO_2 synthesized by a sol–gel Synthesis was a more efficient photocatalyst for the photocatalytic decomposition of rhodamine-6G than TiO_2 alone [38]. Also, SiO_2 incorporated with Fe_3O_4 and used for preparing functional nanocomposites (Fe_3O_4/SiO_2/GMA/AN) by γ-irradiation increases the adsorption of basic

violet 7 dye [39]. A core–shell Fe_3O_4@SiO_2 nanocatalyst was prepared for Fenton-like degradation of malachite green dye [40]. The increase in efficiency was attributed to the presence of SiO_2.

In this study, gamma radiation synthesizes of PVA-co-AAm copolymer and poly(vinyl PVA-co-AAm /TiO_2/SiO_2 nanocomposites were obtained by polymerization of PVA and AAm in presence of TiO_2/SiO_2 nanopowders at different irradiation doses for possible applicability as novel and efficient adsorbents for removal and adsorption of Cu (II) ions and BB3from their aqueous solutions. FTIR, XRD, SEM, EDS, TEM, and DLS characterized the obtained nanocomposites. The batch adsorption experiments by studying the effect of a variety of conditions like contact time, pH of the solution, initial concentration, adsorbent dosage, and temperature on adsorption of BB3 or Cu (II) ions were performed. The experimental data were estimated using adsorption kinetics, adsorption isotherm models, and thermodynamic studies and parameters concerning temperature dependence were also applied.

2 Experimental

2.1 Materials

Acrylamide (CH2=CHC (O) NH_2) (AAm) 97%, was obtained from Pratap Chemical Industries, India. Poly(vinyl alcohol) $[CH_2CH(OH)]_n$ (PVA) of molecular weight 17–18 kDa and 87–89% degree of hydrolysis, Copper chloride ($CuCl_2$) 97%, hydrochloric acid (HCl) (36.5%), sodium hydroxide (NaOH) were obtained from Qualikemes fine chemicals Pvt. Ltd. New Delhi, India, Titanium dioxide (TiO_2) nanopowder (particle size < 25 nm and purity 99.7%), and silicon dioxide (SiO_2) nanopowder of 10–20 nm particle size and purity 99.5% were supplied from Sigma Aldrich Chemie, GmbH, Germany. Astrazon blue BG-200% or basic blue 3 (BB3) ($C_{20}H_{26}ClN_3O$) was supplied by Dystar company, Cairo, Egypt.

2.2 Radiation Synthesis of PVA-co-AAm

The PVA-co-AAm copolymer was synthesized by gamma radiation-induced copolymerization reaction and copolymer compositions of 10 wt%. The reaction mixture was obtained by adding AAm monomer solution (5.0 wt%) to PVA (5.0 wt%) of (50/50) copolymer composition (V/V) under constant stirring for 2 h at a temperature of 50 °C until homogeneity. Then, the PVA/AAm reaction mixtures were cooled to room temperature, deaerated by bubbling with N_2 gas for 3–5 min, sealed, and then subjected to γ-radiation from ^{60}Co Canadian irradiation facility γ-rays at a dose of 30 kGy (dose rate 1.12 kGy/h). The irradiation facility was established at the National Center for Radiation Research and Technology, Egyptian Atomic Energy Authority, Cairo, Egypt. Finally, the obtained PVA-co-AAm-30 copolymer was cut into small discs, immersed in distilled water for 24 h to remove non-reacted materials, and left to dry at 50 °C.

2.3 Radiation Synthesis of PVA-co-AAm/TiO_2/SiO_2 Nanocomposites

The PVA-co-AAm/TiO_2/SiO_2 nanocomposites were synthesized by sonochemical and gamma radiation-induced copolymerization techniques as follows: 0.25 g of TiO_2 and 0.25 g of SiO_2 nanopowders were added to the PVA/AAm reaction mixture solution as prepared above under constant stirring at 50 °C for 2 h. After the reaction mixture (PVA/AAM/TiO_2/SiO_2) was homogenized, the mixture was sonicated for an extra 2 h using ultrasonic (70 w) for full dispersion of TiO_2/SiO_2 nanopowders. The use of ultrasonic produces a variety of compounds with adjustable dimensions and shapes. Then, the PVA/AAM/TiO_2/SiO_2 reaction mixtures were cooled to room temperature, placed into test tubes, deaerated by bubbling with N_2 gas for 5 min, sealed, and then exposed to γ-radiation from ^{60}Co Canadian irradiation facility γ-rays at different doses of 10, 30 and 50 kGy (dose rate 1.12 kGy/h). The obtained PVA-co-AAm/TiO_2/SiO_2 nanocomposites were washed well with ethanol to eliminate unreacted materials, dried at 50 °C, and then ground in a mortar to a fine powder for further use and analysis. According to the irradiation dose, PVA-co-AAm/TiO_2/SiO_2 nanocomposites in which the nanocomposite irradiated with 10, 30 and 50 kGy named PVA-co-AAm/TiO_2/SiO_2-10, PVA-co-AAm/TiO_2/SiO_2-30 and PVA-co-AAm/TiO_2/SiO_2-50 nanocomposites, respectively.

2.4 The Gelation(%)

The dried PVA-co-AAm and PVA-co-AAm/TiO_2/SiO_2 nanocomposites of known weights (W_i) were soaked at 70 °C in deionized water for 24 h to eliminate the insoluble parts. Then, dried to a constant weight (W_d). The gelation(%): established according to Eq. (1):

$$Gelation(\%) = \frac{(W_d)}{(W_i)} \times 100 \quad (1)$$

2.5 Swelling(%)

Known weights (W_d) of dried PVA-co-AAm and PVA-co-AAm/TiO_2/SiO_2 nanocomposites were immersed in distilled water at room temperature until the equilibrium swelling was obtained after 24 h. Then, samples were weighed (*Ws*)

after removing the excess water on their surfaces by a filter paper. The swelling(%) was estimated according to Eq. (2):

$$Swelling(\%) = \frac{(W_s - W_d)}{(W_d)} \times 100 \quad (2)$$

2.6 Batch Experiments for Uptake of BB3 or Cu (II) Ions

The effect of the prepared PVA-co-AAm-30 copolymer and PVA-co-AAm/TiO_2/SiO_2-10, PVA-co-AAm/TiO_2/SiO_2-30, PVA-co-AAm/TiO_2/SiO_2-50 nanocomposite as an adsorbent on the adsorption and removal of BB3 or Cu (II) ions as adsorbates were studied by adding an appropriate amount of 0.2 g of each adsorbent to 50 ml of the aqueous solution of dye or Cu (II) ions with initial concentration 200 mg/L at room temperature for 2 h with shaking at an agitation speed of 100 rpm. Then, the decrease in UV absorbance was measured using T60 UV/Vis spectrophotometer from PG instruments limited to select the better adsorbent for further batch adsorption experiments. According to the results obtained from Table 1 and Fig. 5, the PVA-co-AAm/TiO_2/SiO_2-30 nanocomposite shows high swelling(%) and a higher impact on decreasing the absorbance value of dye or Cu (II) ions, therefore, it was selected for further batch adsorption experiments.

The factors affecting the removal(%) and the adsorption capacity of BB3 or Cu (II) ions by PVA-co-AAm/TiO_2/SiO_2-30 nanocomposite were examined at various experimental conditions using 50 ml volume of dye or metal ions solutions and time intervals up to 24 h as follows: (i) the effect of initial concentration (100–250 mg/L), (ii) the effect of adsorbent amount (0.1–0.4 g), (iii) the effect of pH (4, 7, 9 and 11 for dye; and 3, 4.5 and 6 for Cu (II) ions) and (iv) the effect of temperature (298, 308 and 318 K). After each experiment, the concentration of dye was determined by measuring its absorption at λ_{max} = 654 nm by using T60 UV/Vis spectrophotometer from PG instruments limited.

Table 1 The impact of irradiation dose on gelation(%) and swelling(%) of PVA-co-AAm-30 and PVA-co-AAm/TiO_2/SiO_2 nanocomposites

Sample key	Dose (kGy)	Gelation(%)	Swelling(%)
PVA-co-AAm-30	30	89.6	204.3
PVA-co-AAm/TiO_2/SiO_2-10	10	90.8	165.5
PVA-co-AAm/TiO_2/SiO_2-30	30	93.1	197.7
PVA-co-AAm/TiO_2/SiO_2-50	50	95.7	143.6

The remaining Cu (II) ions concentration in the feed solution after adsorption was determined with atomic absorption spectrometer (AAS)—Thermo scientific iCE 3000 series (AA) Spectrometer, Cambridge, England. The batch experiments were carried in triplicate. The calculation of adsorbed capacity (q_e) at equilibrium and the amount adsorbed (q_t) at time intervals was determined utilizing Eqs. 3, 4:

$$Amountadsorbed(q_e) = \frac{(C_o - C_e) \times V}{m} \quad (3)$$

$$Amountadsorbed(q_t) = \frac{(C_o - C_t) \times V}{m} \quad (4)$$

The removal(%) was calculated using Eq. 5:

$$Removal(\%) = \frac{(C_o - C_e)}{C_o} \times 100 \quad (5)$$

where C_0, C_t, and C_e are the initial concentrations of dye or metal ions (mg/L) before adsorption, the concentration at time (t), and the concentration at equilibrium, respectively, m is the weight of dry adsorbent (g).; V is the volume of the aqueous dye or metal ions solution (L).

2.7 Adsorption Isotherms

Adsorption isotherms at equilibrium were carried out in a 50 ml solution of an initial concentration of 150 mg/L of BB3 and 200 mg/L of Cu (II) ions with 0.4 g adsorbent dosage of PVA-co-AAm/TiO_2/SiO_2-30. The mixture was constantly agitated at 100 rpm at different temperatures of 298, 308, and 318 K. The concentrations of dye or Cu (II) ions were measured, and the data obtained were analyzed with the Langmuir, Freundlich, and Temkin isotherm models.

2.8 Adsorption Kinetics

Adsorption kinetic at equilibrium studies were carried out in a 50 ml solution of an initial concentration of 50, 100, 150, and 200 mg/L of BB3 and 150 mg/L of Cu (II) ions with 0.3 g adsorbent dosage of PVA-co-AAm/TiO_2/SiO_2-30 at temperature 298 K. The concentrations of BB3 or Cu (II) ions were measured at a varied time intervals between 0 and 600 min. The data obtained were analyzed using pseudo-first-order pseudo-second-order and intra-particle diffusion kinetic models.

2.9 Adsorption Thermodynamics

Adsorption of BB3 or Cu (II) ions was investigated at various temperatures of 298, 308, and 318 K in a water bath shaker at 100 rpm agitation speed at equilibrium using a

50 ml solution of an initial concentration of 150 mg/L of BB3 and 200 mg/L of Cu (II) ions with 0.4 g adsorbent dosage of PVA-co-AAm/TiO_2/SiO_2-30. The enthalpy (ΔH^0), entropy (ΔS^0), and Gibbs free energy (ΔG^0) were thermodynamic parameters employed to determine the nature and spontaneity of the adsorption process.

2.10 Characterization Analysis

The chemical structure of the nanocomposites was analyzed by ATR-FTIR spectroscopy, Bruker Optik GmbH, Ettlingen, Germany. XRD-600 instrument with Ni filter and Cu-Kα supplied From Shim Kyoto, Japan, used to obtain X-ray diffraction curves. The surface morphology of the copolymers and nanocomposites was investigated with SEM, JEOL JSM-5400, Japan. Energy dispersive spectrometry (EDS) analysis LINK'S (Oxford Instruments link ISIS, UK) connected to scanning electron microscope model JEOL JSM-5400 (Japan) was used to perform the consisting of the peaks belonging to the C, O, Si and Ti. The particle size and distribution examined using a Transmission Electron Microscopy (TEM), JEOL JSM–100 CX, Japan, with an acceleration voltage of 80 kV. The distribution of particle of PVA-co-AAm/TiO_2/SiO_2-30 kGy nanocomposite was performed by dynamic light scattering (DLS-ZP/Particle Sizer Nicomp 380ZLS), USA. The effect of nanocomposites on the dye concentration was determined by measuring its absorption at $\lambda_{max} = 654$ nm by utilizing the T60 UV/Vis spectrophotometer from PG instruments limited. The remaining Cu (II) ions concentration in the feed solution after adsorption was determined with atomic absorption spectrometer (AAS)—Thermo scientific iCE 3000 series (AA) Spectrometer, Cambridge, UK.

3 Results and Discussion

3.1 The Effect of Irradiation Dose on Gelation(%) and Swelling(%)

Gamma irradiation is a useful crosslinking polymerization technique over other chemical crosslinkers and an effective method to prepare polymeric-based nanocomposite. In this study, the copolymer prepared at 30 kGy (PVA-co-AAm-30) and three PVA-co-AAm/TiO_2/SiO_2 nanocomposites were prepared using the gamma irradiation technique at different doses of 10, 30, and 50 kGy. Table 1 illustrated the effect of irradiation dose on gelation(%) and swelling(%) of PVA-co-AAm-30 copolymer and PVA-co-AAm/TiO_2/SiO_2 nanocomposites. The increase in irradiation dose from 10 to 50 kGy doses does not lead to a significant increase in gelation(%). The gelation(%) was in the range of 90.8 to 95.7%. This is due to increasing the cross-linking reaction between PVA-co-AAm upon the effect of the gamma irradiation. Also, PVA-co-AAm/TiO_2/SiO_2-30 had the highest swelling(%) of 197.7% then decreases at 50 kGy due to the increase in cross-linking density.

3.2 Characterization Analysis

3.2.1 FT-IR Investigation

Figure 1 illustrates the FT-IR spectrum of PVA, AAm, and the as-synthesized nanocomposite. The spectrum of PVA (Fig. 1a) demonstrates peaks at 3290/cm and 2923/cm related to the –OH and C–H alkyl, respectively. Stretching vibration peaks correspond to C–O, and C=O from residual ester groups appear at 1437/cm and 1728/cm, respectively. Also, the stretching vibrations peaks characteristic to C–O and C–O–C appear at 1024/cm and 1092/cm, respectively [41].

The FTIR spectrum of AAm Fig. 1b shows the peaks at 1610/cm and 1668/cm corresponding to the bending vibration of the $–NH_2$ group and stretching vibrations of the –C=O group, respectively. The peaks at 1426/cm and 1476/cm resulted from the scissor and bending vibrations of CH–CO and $–CH_2$ groups, respectively. Additionally, the absorption peak attributed to the stretching vibrations of $–CH_2$ appears at 2975 and 2811/cm. A broad absorption band resulted from the –NH group that appeared at 3184/cm and 3348/cm. Finally, the absorption stretching vibration band from C–N group resulted at 1350/cm while the broad absorption bands resulted from the out-of-plane bending vibration of the NH_2 group appears in the range of 619–655/cm were.

The FT-IR spectrum of PVA-co-AAm/TiO_2/SiO_2 nanocomposite (Fig. 1c) shows stretching vibration peaks characteristic to the C=O of amide I and N–H bending vibration at 1720/cm and 1668/cm, respectively. Moreover, a minor peak shift and broadening appeared at 3340/cm due to the overlapping of –NH groups of AAm and –OH of PVA stretching vibrations forming a hydrogen bonding between them. These results indicated the successful grafting of AAM onto the PVA backbone [42]. The stretching vibration peaks related to the Ti–O–Ti resulted in the range 557–752/cm. The asymmetric stretching vibrations absorption bands of Si–O–Si appeared at 1127 and 1058/cm and a peak at 490/cm that corresponding to Si–O–Si bending vibration [43] and Si–O–H appeared at 993 –927/cm.

3.2.2 XRD Studies

X-ray diffraction is an important tool, which provides the crystallinity and lattice structure of nanocomposite. Figure 2 shows the XRD patterns and the crystalline structure of PVA-co-AAm-30, and PVA-co-AAm/TiO_2/SiO_2

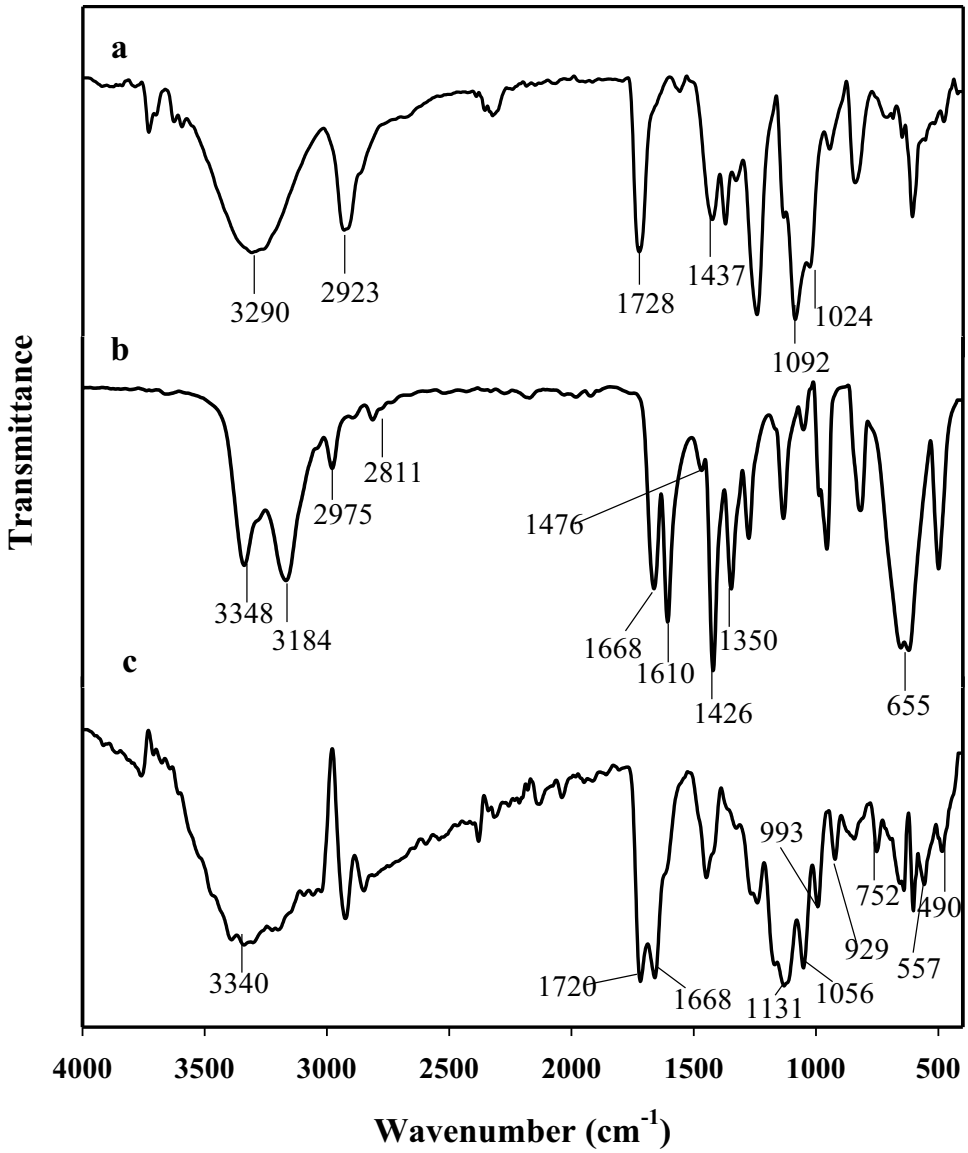

Fig. 1 FTIR spectra of **a** PVA, **b** AAm and **c** PVA-co-AAm/TiO_2/SiO_2 nanocomposite

nanocomposites prepared at different doses of 10, 30, and 50 kGy. Figure 2a shows XRD of PVA-co-AAm-30 showed semi-crystalline peaks at the 2θ = 19.1° [44]. The XRD curves of PVA-co-AAm/TiO_2/SiO_2 nanocomposite prepared at different doses of 10, 30 and 50 kGy (Fig. 2b–d) illustrate the same diffraction peaks of PVA-co-AAm-30 with a small shift at 2θ = 19.1° which is attributed to the presence of TiO_2 and SiO_2 in addition to the diffraction peak of SiO_2 overlapped with the diffraction peak of PVA-co-AAm-30 at 2θ = 19.1°. The characteristic peaks of TiO_2 nanoparticles observed at 2θ = 25.1°, 37.6°, 47.9°, 53.7°, 55.1°, 62.6°, 68.3°, 69.9° and 74.9° which confirms the spinal structure of the Bragg reflections of anatase phase of TiO_2 nanoparticles corresponding to the crystal planes of the (A101), (A004), (A200), (A105), (A211), (A118), (A116) and (A220), respectively [45]. In addition, the peaks at 27°, 36.2° and 55.0° corresponding to the crystal planes of the (R110), (R101), and (R211) which corresponds to TiO_2 in the rutile phase.All peaks are well in agreement with the standard spectrum (JCPDS No.: 21-1272, 88-1175 for rutile, and 84-1286 for anatase) [46]. In the XRD spectra, the characteristic peak at 2θ = 25.10° and 27.0° signifies the existence of TiO_2, which compatible with the composition of 80% anatase and 20% rutile as the same results in the previously reported study [47]. The majority structure of TiO_2 in anatase phase candidate their possible use as an effective adsorbent for the adsorption process of metal ions and dyes.

The average crystallite size of the as-prepared nanocomposites was determined from Debeys–Scherrer Eq. (6)

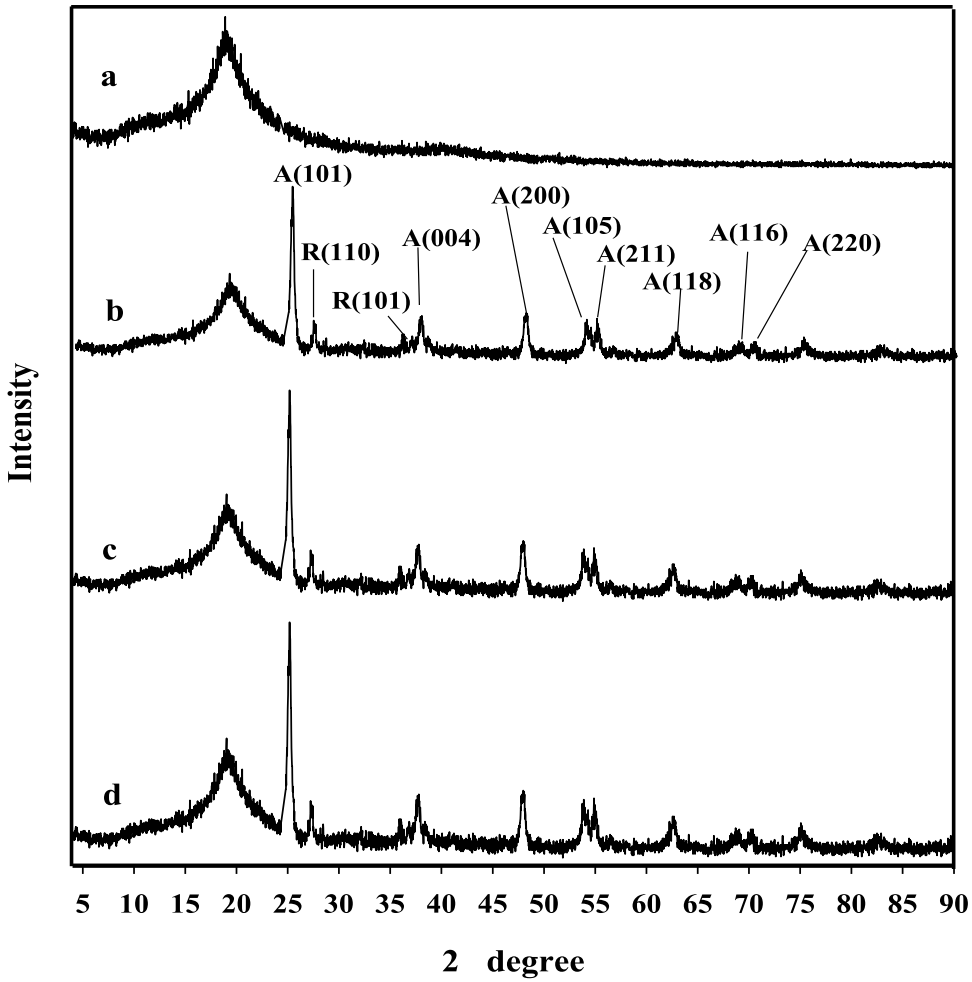

Fig. 2 XRD curves of **a** PVA-co-AAm, **b** PVA-co-AAm/TiO_2/SiO_2-10 **c** PVA-co-AAm/TiO_2/SiO_2-30 and **d** PVA-co-AAm/TiO_2/SiO_2-50 nanocomposites

Table 2 The crystalline size (D) of XRD data calculated using the Debye–Scherrer formula

2θ	θ	Cos θ	FWHM (radion)	β	D (nm)
19.1	9.56	0.9861	0.36	0.0036	39.1
25.1	12.55	0.9761	0.4327	0.004224	32.8
27.0	13.5	0.9724	0.305	0.002966	46.7
36.2	18.1	0.9505	0.31	0.002947	47.1
37.6	18.5	0.9483	0.45	0.004267	32.5
47.9	23.95	0.9139	0.5267	0.004814	28.8
53.7	26.85	0.8922	0.36	0.003212	43.1
55.1	27.55	0.8870	0.5153	0.004571	30.3
62.6	31.3	0.8544	0.48	0.004101	33.8
68.3	34.15	0.8276	0.24	0.001986	69.8
69.9	34.95	0.8196	0.24	0.001967	70.5
74.9	37.45	0.794	0.44	0.003493	39.7

$$D = \frac{k\lambda}{\beta \mathrm{Cos}\theta} \tag{6}$$

where D is particle diameter size, k is the so-called shape or geometry factor which equals 0.9, λ is the x-ray wavelength ($\lambda = 0.1541$ nm), β is the full width at half maximum (FWHM) of diffraction peak and θ is the diffraction angle. The XRD data of peaks details and the average particle size (D) calculated using the Debye–Scherrer formula as presented in Table 2. The calculated average crystallite size of the as-synthesized product was about 43 nm. The average crystalline size was previously calculated using the Debye–Scherrer formula in different studies [48, 49].

3.2.3 TEM and DLS Analysis

Figure 3 shows TEM images of PVA-co-AAm/TiO_2/SiO_2 nanocomposites prepared at different irradiation doses of 10, 30, and 50 kGy. Generally, bright images of TiO_2 and SiO_2 nanoparticles with spherical shape embedded in a gray shell of PVA-co-AAm molecules with an average size of 60–70 nm. In addition, the TiO_2 and SiO_2 nanoparticles were dispersed well of good uniform distribution with no agglomeration. It was noticed that the irradiation dose affects TEM results. With increasing the irradiation dose during the preparation of nanocomposite, the high dispersion of TiO_2/SiO_2 nanoparticles

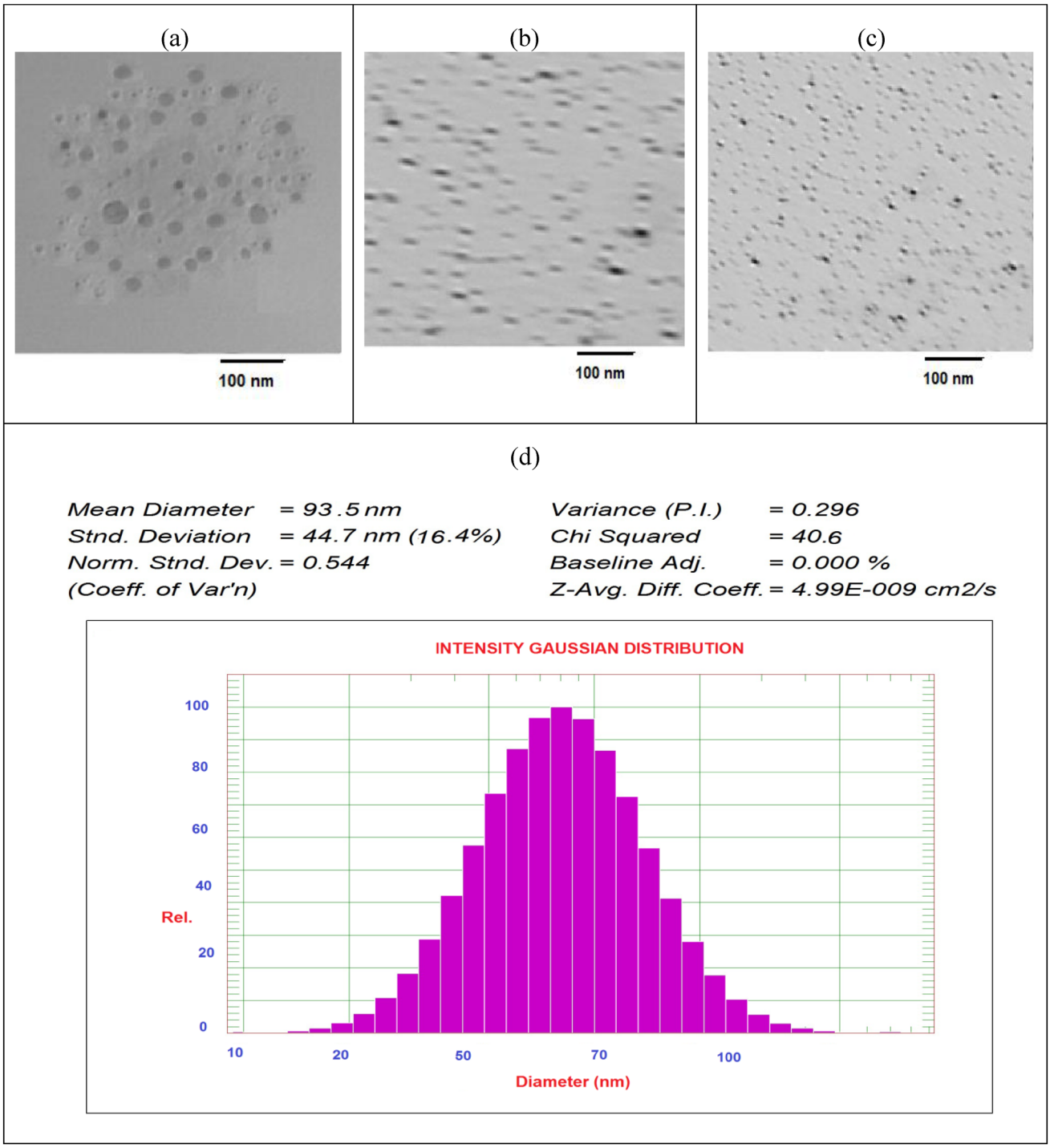

Fig. 3 TEM images of **a** PVA-co-AAm/TiO_2/SiO_2-10, **b** PVA-co-AAm/TiO_2/SiO_2-30 and **c** PVA-co-AAm/TiO_2/SiO_2-50. **d** DLS of PVA-co-AAm/TiO_2/SiO_2-30 nanocomposite

inside the nanocomposite especially that prepared at 50 kGy (Fig. 3c). The particle size distribution of PVA-co-AAm/TiO_2/SiO_2-30 (Fig. 3d) obtained from DLS was homogeneously shaped with an average size of about 93.5 nm which is large and nearly close to the TEM characterization due to the association and aggregation molecules of nanocomposite in aqueous media via Vander Waal's force or hydrogen bonding.

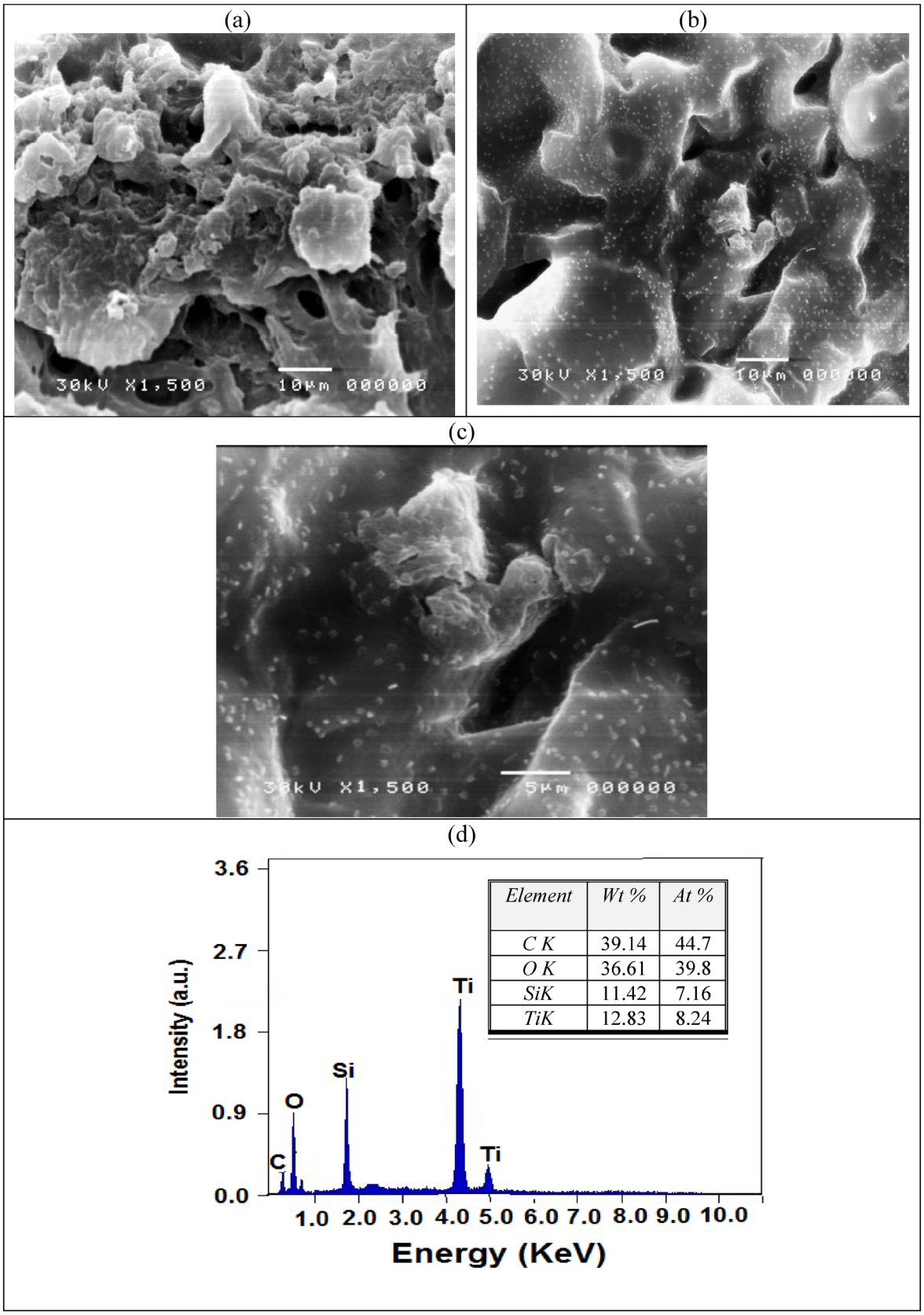

Fig. 4 SEM micrographs of **a** PVA-co-AAm/TiO_2/SiO_2-10 **b** PVA-co-AAm/TiO_2/SiO_2-30 and **c** PVA-co-AAm/TiO_2/SiO_2-50. **d** SEM/EDS spectrum of PVA-co-AAm/TiO_2/SiO_2-30 nanocomposite

3.2.4 SEM and EDX Analysis

Figure 4 shows the changes in surface morphology of PVA-co-AAm/TiO_2/SiO_2 nanocomposites investigated by SEM. Figure 4a shows SEM micrograph of PVA-co-AAm/TiO_2/SiO_2-10 had a rocky shape, possess a highly porous structure with white spots, and tightly packaged on the back-scattered image seem to agglomerate particle coated composite surface. While SEM of PVA-co-AAm/TiO_2/SiO_2-30 (Fig. 4b) and PVA-co-AAm/TiO_2/SiO_2-50 (Fig. 4c) has coarse surface and in close contact with one another due to increasing the crosslinking of PVA-co-AAm and the formation of semi-interpenetrating crosslinked network. In addition, the TiO_2/SiO_2 nanoparticles are well distributed on their surfaces. To confirm the presence of all the mentioned elements including Si, Ti, C, and O in the synthesized nanocomposites, elemental analysis was performed on the sample using EDS analysis. Figure 4d demonstrates the EDX analysis of PVA-co-AAm/TiO_2/SiO_2 nanocomposite consisting of the peaks belonging to the C, O, Si and Ti were exactly determined. The most intense peak of C is originated from PVA and AAm. O is originated from PVA, AAm, TiO_2, and SiO_2. The result revealed that Ti is detected at 4.5–5.0 keV and Si is detected at 1.8 keV.

3.3 Uptake of Dye and Heavy Metal Ions

3.3.1 Effect of Adsorbent Composition

It is well known that the adsorbent composition plays a crucial role in the adsorption of metal ions and dyes. Thus, the enhancement of the metal or dye adsorption capability of PVA-co-AAm by incorporation of TiO_2/SiO_2 nanoparticles was investigated. Figure 5 shows the change in UV absorbance of BB3 and Cu (II) ions after treatment by PVA-co-AAm-30 and the as-synthesized PVA-co-AAm/TiO_2/SiO_2 nanocomposites. The absorption intensity value of BB3 and Cu (II) ions solution decreased upon the treatment by the as-synthesized PVA-co-AAm/TiO_2/SiO_2 nanocomposites. The results confirm that PVA-co-AAm/TiO_2/SiO_2 nanocomposites enhance and provide better adsorption capacities of both dye and metal ions compared to PVA-co-AAm-30. From the results of Fig. 5, the adsorption efficiency(%) of PVA-co-AAm-30, PVA-co-AAm/TiO_2/SiO_2-10, PVA-co-AAm/TiO_2/SiO_2-50 and PVA-co-AAm/TiO_2/SiO_2-50 towards the adsorption of BB3 after 2 h of reaction time was 19.1, 54.8, 60.3, 62.6%, respectively and the adsorption efficiency(%) towards the adsorption of Cu (II) ions after 2 h of reaction time was 27.3, 56.8, 68.1 and 71.4%, respectively.

The synergy of adsorption significantly improved by the presence of TiO_2/SiO_2 nanoparticles and the amount of uptake of dye or Cu (II) ions increased about three-folds rather than copolymer. This is due to the reactive surface and large specific area of TiO_2/SiO_2 nanoparticles and due to the presence of active sites like hydroxyl groups of PVA and amido groups of AAm on the adsorbent that facilitates the adsorption of dye and metal ions through hydrogen bond formations and electrostatic interactions.

In addition, it was noticed that the PVA-co-AAm/TiO_2/SiO_2-30 and PVA-co-AAm/TiO_2/SiO_2-50 showed the highest adsorption capacity. However, PVA-co-AAm/TiO_2/SiO_2-30 shows high swelling(%) as the results obtained from Table 1, and therefore it was selected for further adsorption experiments. The modification of the surface characteristics of TiO_2 and SiO_2 to adsorb effectively the special colored organic molecules was studied previously for degradation of Rhodamine B [50] and for removal of volatile organic compounds [51], Also, PVA and AAm were polymerized in various formulations by different techniques as an effective adsorbent for adsorption of metals ions [5] or dye [12].

3.3.2 Effect of pH

The effect of initial pH (4, 7, 9, and 11) and pH (3, 4.5, and 6) on the adsorption capacity and removal(%) of BB3 and Cu (II) ions, respectively by PVA-co-AAm/TiO_2/SiO_2-30 nanocomposite as a function of various contact time up to 24 h was investigated in Fig. 6. Generally, the removal(%) of Cu (II) ions and BB3 increased as the pH increases. Also, the removal(%) for the adsorbed dye (Fig. 6a) or Cu (II) ions (Fig. 6b) increases as the contact time increases and reaches the equilibrium adsorption after 7 h for BB3 and 6 h for Cu (II) ions. However, as the contact time increased to 24 h, the amount of both dye and Cu (II) ions adsorbed onto the nanocomposite surface increases slightly. This is owing to the saturation of available surface sites of the nanocomposite. Therefore, the optimized pH for high adsorption was noticed at pH 11.0 for BB3 and 6.0 for Cu (II) ions for the next batch experiments. The removal(%) for BB3 and Cu (II) ions was and 92.1 and 95.4% at the optimum pH, respectively.

Figure 6b shows that the adsorption of Cu (II) was profoundly dependent on pH since pH influences the solubility of Cu (II) ions and the ionization state of the -OH and $–CONH_2$ groups in the PVA-co-AAm/TiO_2/SiO_2-30 nanocomposite. In addition, the increase in pH Cu (II) ions (>6.0) was restricted to avoid the creation of copper hydroxide. The adsorption of the BB3 and Cu (II) ions is low at pH <6. This demonstrates that the solution acidity reduces the BB3 and Cu (II) ions' adsorption. This behavior could be explained based on the change in the surface charge of PVA-co-AAm/TiO_2/SiO_2-30 nanocomposite. In acidic solution, the active groups of PVA-co-AAm/TiO_2/SiO_2-30 nanocomposite such as hydroxyl and amide groups are protonated and competition between H^+ and both BB3 and Cu (II) ions for adsorption sites led to little adsorption of metal ion or dye. Meanwhile, as the pH increases, deprotonation of the

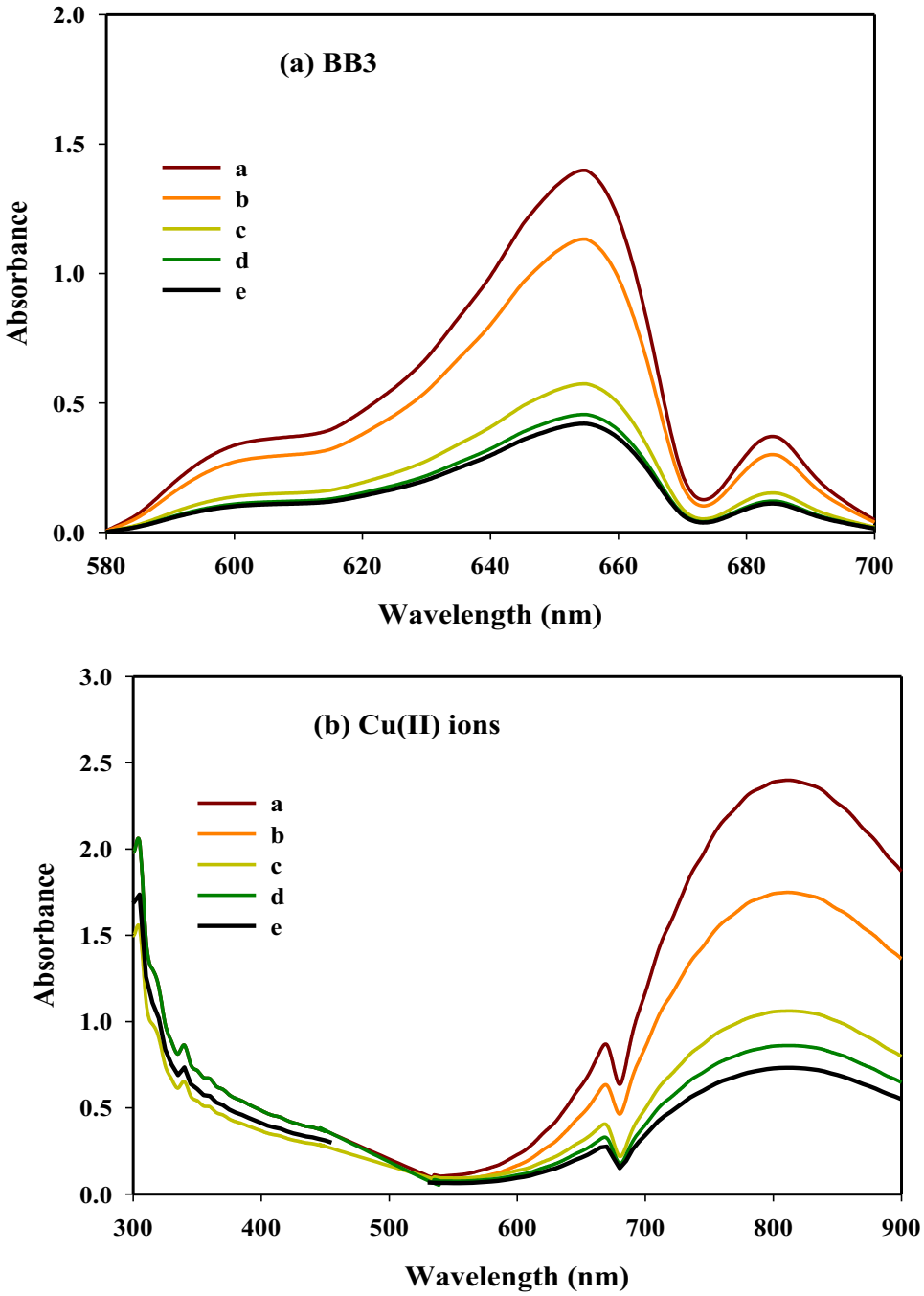

Fig. 5 The change in UV absorption spectra of (A) BB3 and (B) Cu (II) ions after treatment by the as-synthesized adsorbent samples, where **a** original solution of dye or Cu (II) ions, **b** PVA-co-AAm-30, **c** PVA-co-AAm/TiO_2/SiO_2-10, **d** PVA-co-AAm/TiO_2/SiO_2-30 and (e) PVA-co-AAm/TiO_2/SiO_2-50. (0.2 g of adsorbent; 50 ml of the aqueous solution of dye or Cu (II) ions with initial concentration 200 mg/L at room temperature for 2 h with shaking at an agitation speed of 100 rpm)

functional groups occur and the PVA-co-AAm/TiO_2/SiO_2-30 nanocomposite surface charge became negative, which prompted advanced adsorption of cationic species. Similar results obtained by Gebru and Das [52] through using cellulose acetate/titanium oxide adsorbents prepared by the electrospinning technique for the removal Cu (II) after 300 min at 35 °C and the highest removal capacities were estimated at pH of 5.8,

3.3.3 Impact of Adsorbent Dosage

The impact of PVA-co-AAm/TiO_2/SiO_2-30 nanocomposite dosage (0.1–0.4 g) on the amount adsorbed of BB3 and Cu (II) ions was considered and the obtained data are presented in Fig. 7. The results demonstrate that the removal efficiency(%) regularly increases as the contact time and adsorbent dosage increase and attained the highest values of 93.5% and 95.2% for BB3 and Cu (II) ions, respectively with adsorbent dosage 0.4 g of PVA-co-AAm/TiO_2/

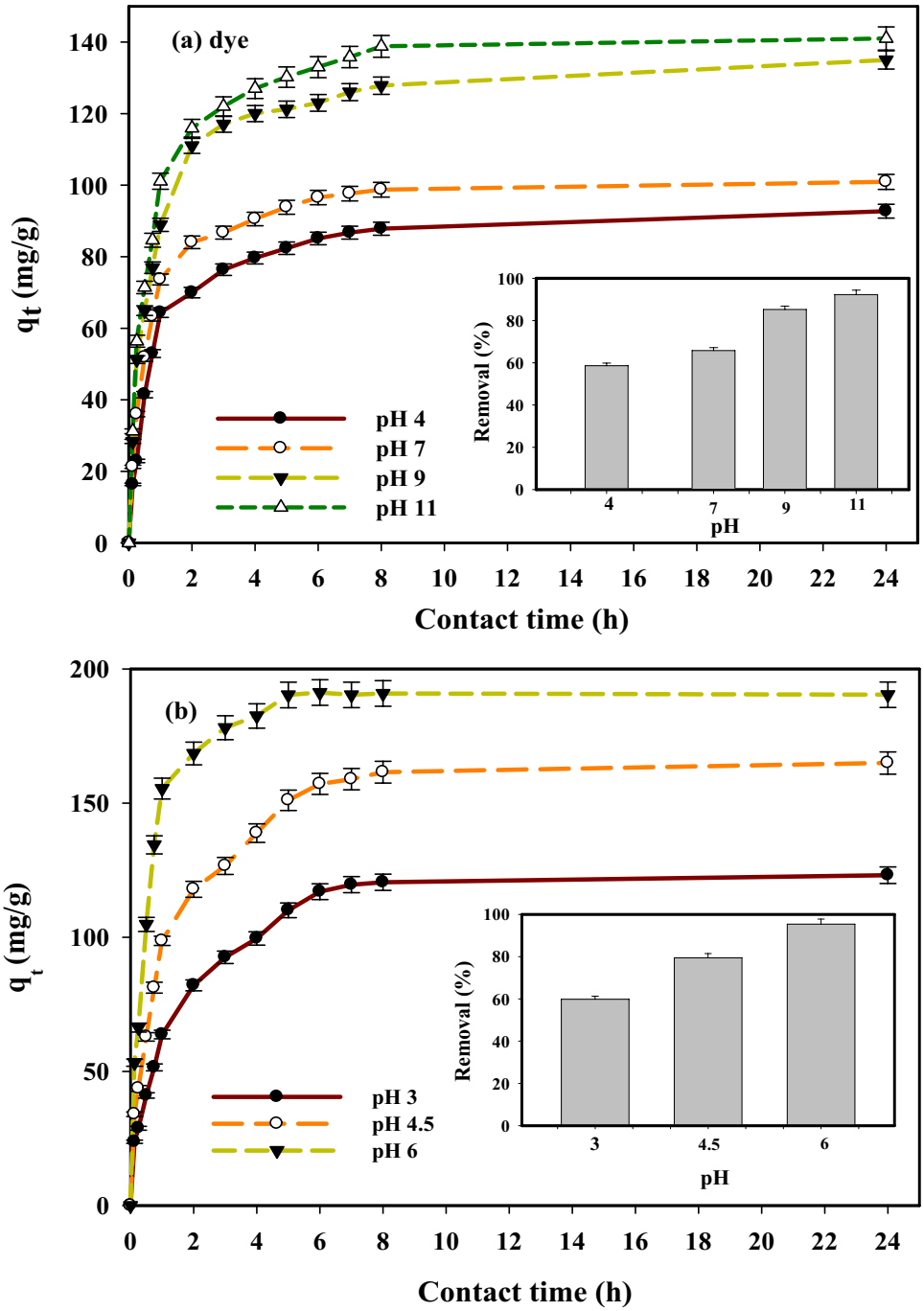

Fig. 6 Effect of pH and contact time (h) on the amount adsorbed (q_t) (mg/g) and removal(%) of **a** BB3 and **b** Cu (II) ions onto PVA-co-AAm/TiO_2/SiO_2 nanocomposite (initial concentration 150 mg/L for the dye and 200 mg/L for Cu (II) ions; adsorbent dosage 0.4 g; temperature 298 K; agitation speed 100 rpm)

SiO_2-30 nanocomposite. However, the saturated removal(%) occurred nearly after a contact time of nearly 7 h for dye and 6 h for Cu (II) ion. Thus, 0.4 g of PVA-co-AAm/TiO_2/SiO_2-30 nanocomposite was chosen to be the optimum dosage for the additional adsorption studies. As the adsorbent mass increases, the adsorption increases that attributed to the increased surface area and consequently the availability of more sites for adsorption. Also, as the contact time increases the adsorption capacity increases, designates that the equilibrium adsorption was about 140.4 mg/g for BB3 and 196.3 mg/g for Cu (II) ions after about 7 h and 6 h contact time, respectively.

Although a wide range of compounds in the literature has been performed as adsorbents or catalysts for removal of organic dye contaminants with the usage of visible radiation like Maijan et al. [12] prepared poly(vinyl alcohol)-*g*-polyacrylamide hydrogel was surface-coated with SiO_2@ZnO nanoparticles (PVA-g-PAM/SiO_2@ZnO) for the removal of methylene blue upon exposure to UV radiation obtained of methylene blue (MB) and the removal was 96% within

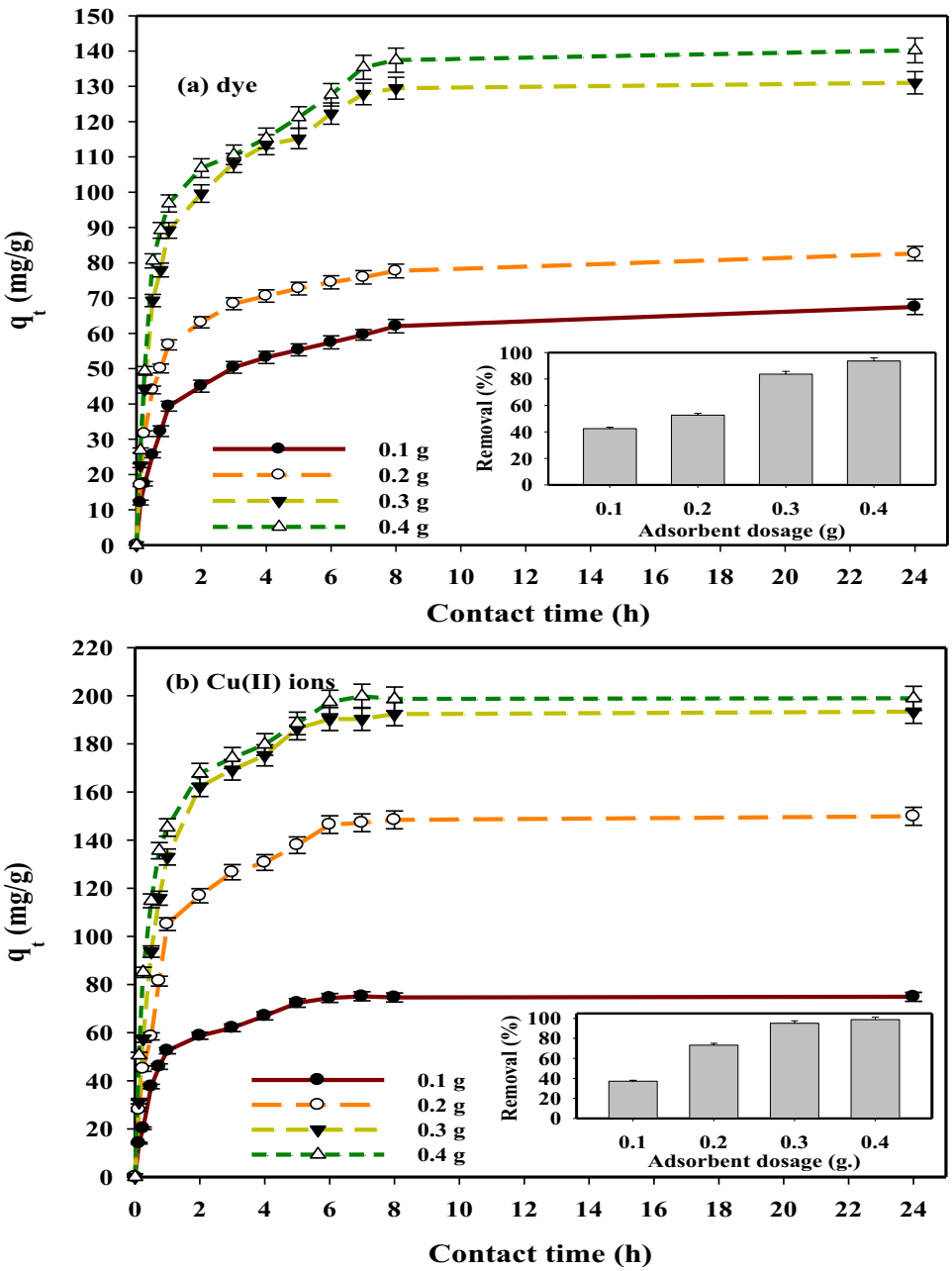

Fig. 7 Effect of adsorbent dosages and contact time (h) on the amount adsorbed (mg/g) of the **a** BB3 and **b** Cu (II) ions onto the PVA-co-AAm/TiO_2/SiO_2-30 nanocomposite (pH 11 for the dye and pH 6 for Cu (II); initial concentration 150 mg/L for the dye and 200 mg/L for Cu (II) ions; temperature 298 K; agitation speed 100 rpm)

24 h. Sakarkar et al. [53] investigate the application of PVA/TiO_2 coated PVDF membrane for the removal of the textile dye under ultraviolet irradiation and the photodegradation was 44.4% for reactive blue, 47.8% for methyl orange, and 45.8% for Rhodamine b for 150 min. Mainly, the removal of dyes using TiO_2 or SiO_2 nanoparticles were achieved under UV radiation however in the present study, the removal of dye or metal ions was achieved by the adsorption technique through the dual effect of the functional hydroxyl and amido groups and TiO_2/SiO_2 nanoparticles in PVA-co-AAm/TiO_2/SiO_2 nanocomposites.

3.3.4 Effect of Initial Concentration

One of the effective parameters on the adsorption efficiency is the initial concentration of metal ions or dye. The effect of initial concentration (100, 150, 200, and 250 mg/L) of BB3 or Cu (II) ions on the adsorption efficiency and removal(%) as a function of various contact times up to 24 h onto the PVA-co-AAm/TiO_2/SiO_2-30 nanocomposite was studied as illustrated in Fig. 8.

The results of adsorption demonstrate that the adsorption capacity and the removal(%) of both BB3 and Cu (II) ions onto the nanocomposite enhanced strongly with the increase in the initial concentration to 150 mg/L for the

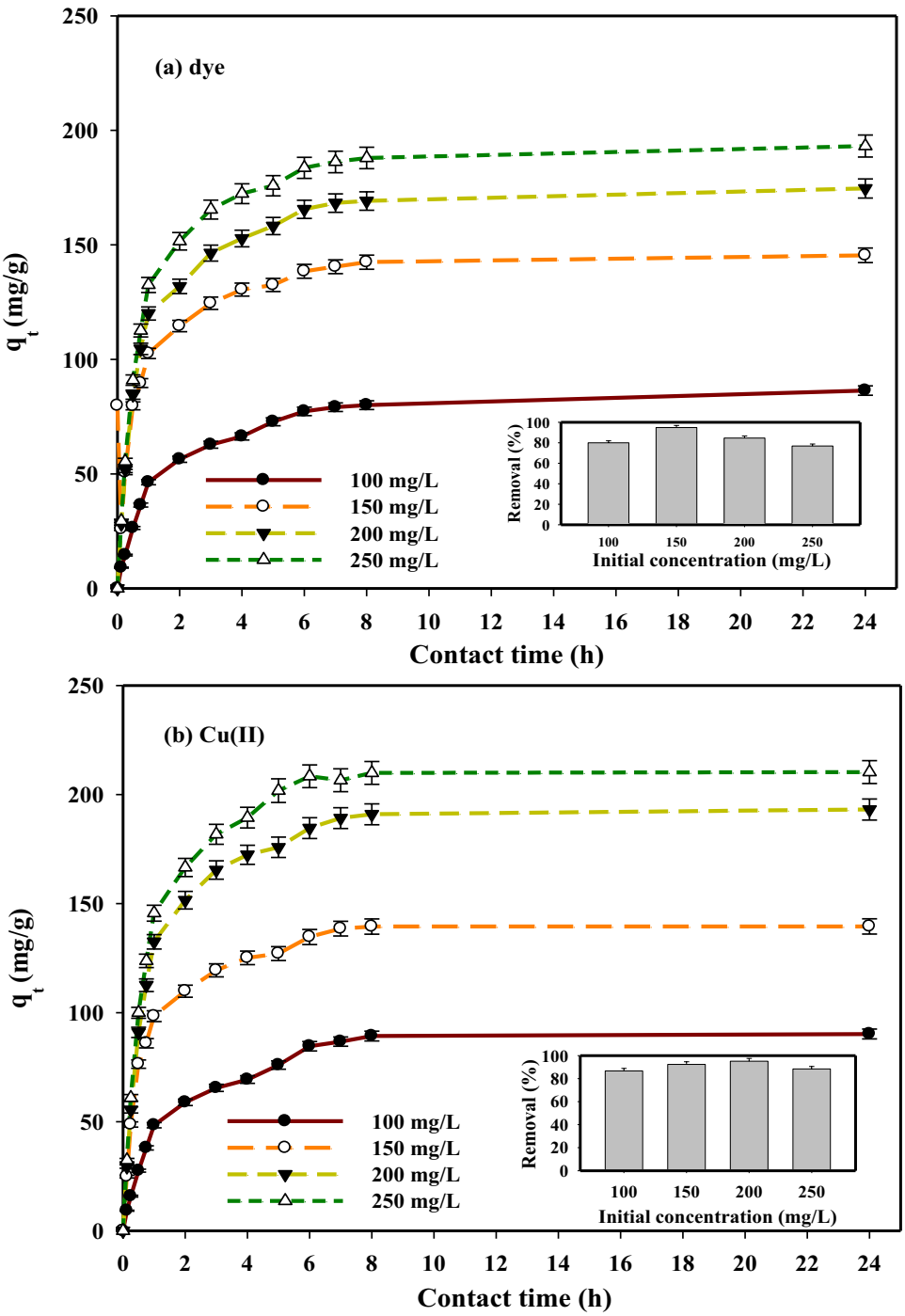

Fig. 8 Impact of initial concentration (mg/l) with contact time (h) onto the amount adsorbed (mg/g) and removal(%) of the **a** BB3 and **b** Cu (II) ions onto the PVA-co-AAm/TiO_2/SiO_2-30 nanocomposite (pH 11 for the dye and pH 6 for Cu (II), 0.4 g adsorbent dosage. temperature 298 K; agitation speed 100 rpm)

BB3 and 200 mg/L for Cu (II) ions. This enhancement in adsorption efficiency may be because of existing adsorption active sites of PVA-co-AAm/TiO_2/SiO_2-30 nanocomposite are available at low initial concentration, thus increasing uptake percentage. At higher concentrations of dye or metal ions, the ratio of the existing surface of nanocomposite to the initial dye or metal ions concentration is minor; consequently, the removal(%) becomes reliant on initial concentrations [54]. However, the adsorption capacity (mg/g) of the dye or the metal ions increased with increasing their initial concentrations. The maximum adsorption capacity of BB3 and Cu (II) ions was noticed at 141.9 and 190.3 mg/g, respectively. From the acquired outcomes, it was apparent that PVA-co-AAm/TiO_2/SiO_2-30 nanocomposite exhibited a strong affinity towards Cu (II) ions than BB3. This is because of the variation in the charge density and the size of the BB3 and Cu (II)

ions. Cu (II) ions have greater charge density and smaller size rather than the BB3 and have a strong attraction to the oxygen and nitrogen atoms lone pair electrons in the hydroxyl and amide groups of nanocomposite forming stable complexes.

3.3.5 Impact of Temperature

Temperature is a significant factor in the strategy of dye or metal ions adsorption and is considered as an important factor to study their thermodynamic behaviors to detect whether the adsorption performance is an exothermic or endothermic reaction. Figure 9 represents the relationship between the temperature dependence and the amount adsorbed (mg/g) or removal(%) of the BB3 and Cu (II)

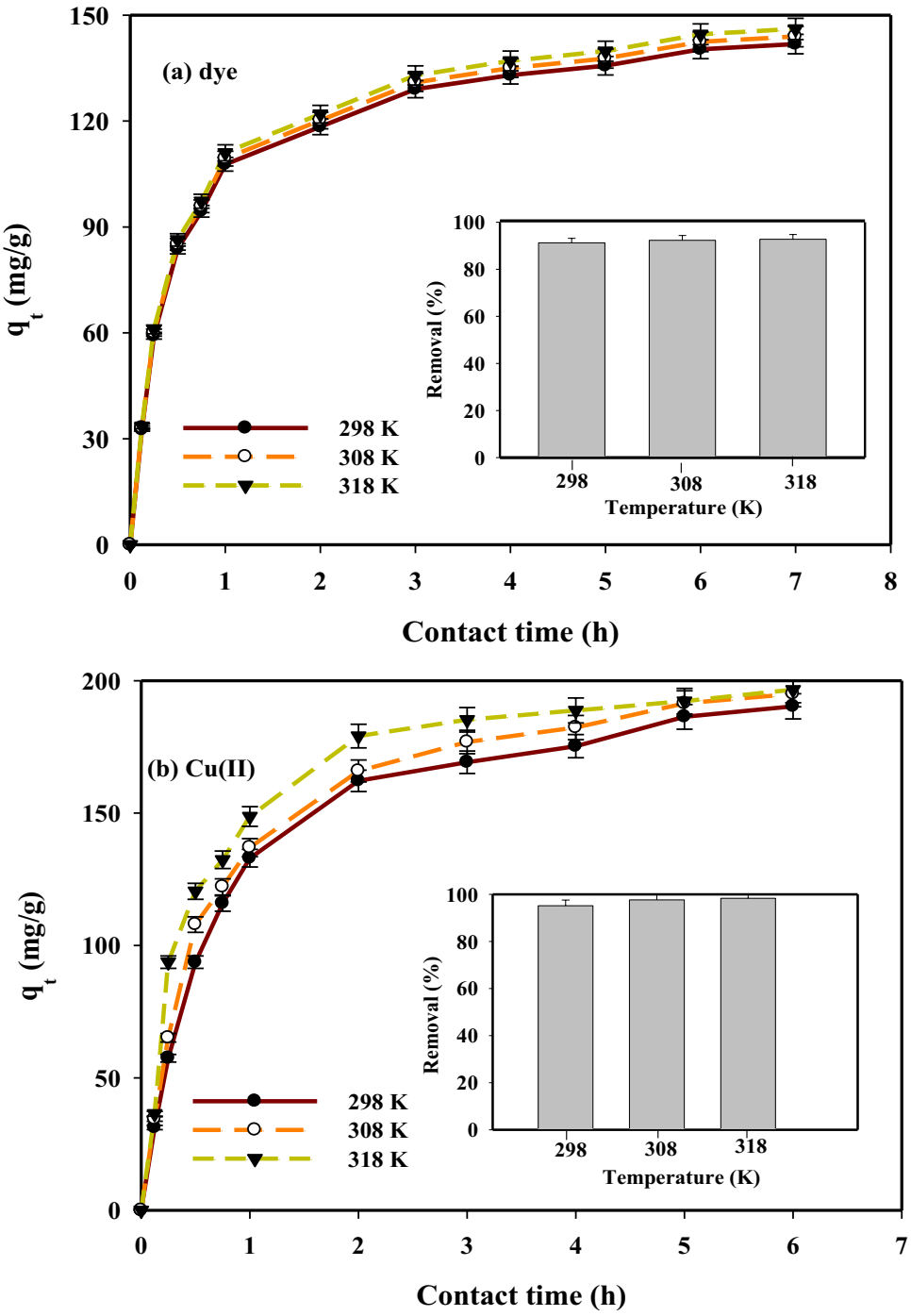

Fig. 9 Impact of temperature (K) with contact time (h) onto the amount adsorbed (mg/g) and removal(%) of the **a** BB3 and **b** Cu (II) ions onto PVA-co-AAm/TiO_2/SiO_2-30 nanocomposite (pH 11 for the dye and pH 6 for Cu (II) ions; contact time 7 h for the dye and 6 h for Cu (II); 0.4 g adsorbent dosage; initial concentration 150 mg/L for the dye and 200 mg/L for Cu (II) ions; agitation speed 100 rpm)

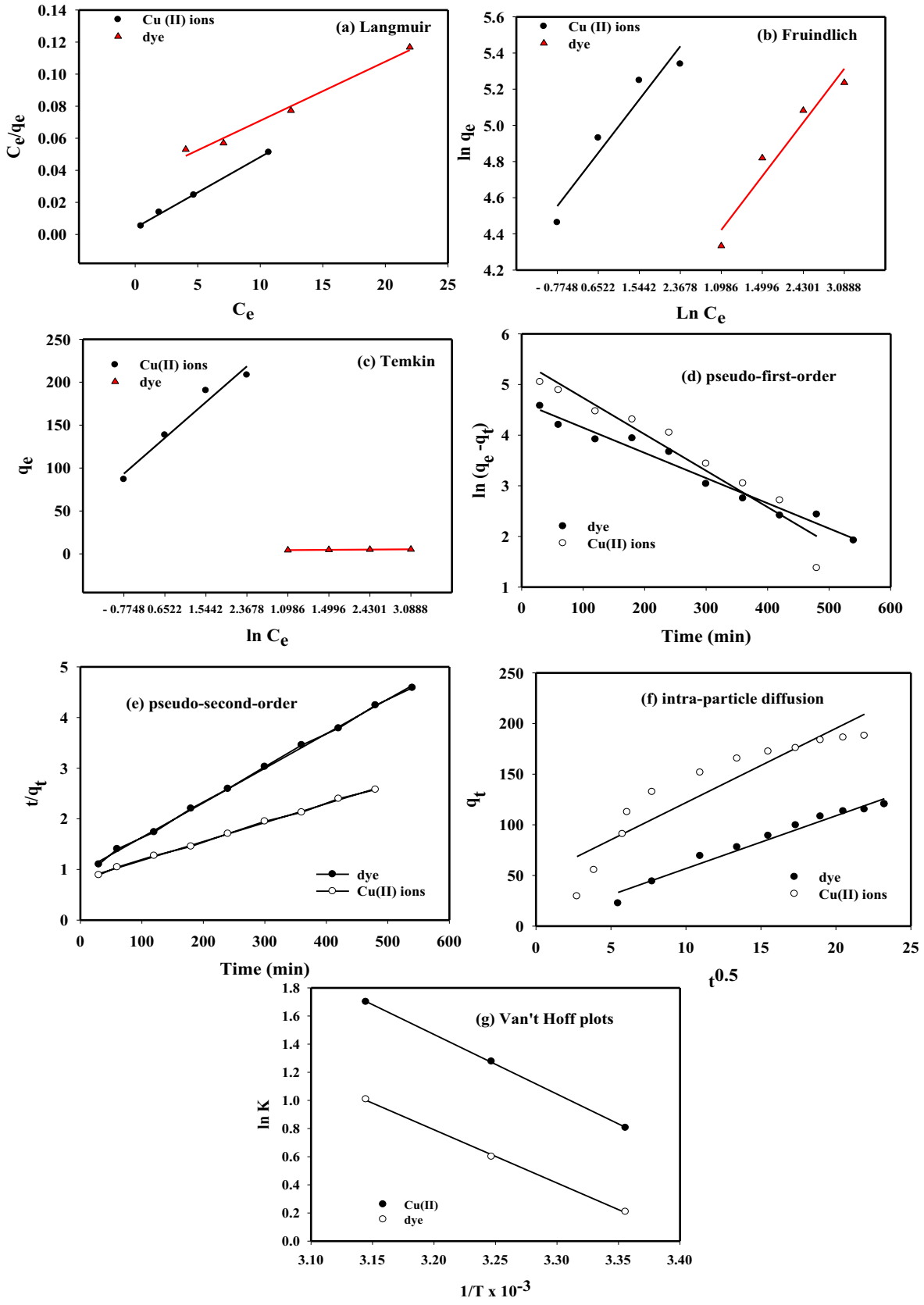
(a) Langmuir
Cu (II) ions
dye
Ce/qe
Ce
(b) Fruindlich
Cu (II) ions
dye
ln qe
- 0.7748 0.6522 1.5442 2.3678 1.0986 1.4996 2.4301 3.0888
Ln Ce
(c) Temkin
Cu(II) ions
dye
qe
- 0.7748 0.6522 1.5442 2.3678 1.0986 1.4996 2.4301 3.0888
ln Ce
(d) pseudo-first-order
ln (qe -qt)
dye
Cu(II) ions
Time (min)
(e) pseudo-second-order
t/qt
dye
Cu(II) ions
Time (min)
(f) intra-particle diffusion
qt
dye
Cu(II) ions
t0.5
(g) Van't Hoff plots
ln K
Cu(II)
dye
1/T x 10-3

◂**Fig. 10** Adsorption isotherm [**a** Langmuir, **b** Freundlich and **c** Temkin models]; adsorption kinetic models [**d** pseudo-first-order, **e** pseudo-second-order and **f** intra-particle diffusion models] and **g** Van't Hoff plots for adsorption of BB3 and Cu (II) ions onto PVA-co-AAm/TiO_2/SiO_2-30 nanocomposite

ions and onto the PVA-co-AAm/TiO_2/SiO_2-30 nanocomposite was performed at 298, 308, and 318 K. It is noticed that the amount of adsorption (mg/g) and removal(%) of both dye and metal ions increase with increasing temperature from 298 to 318 K. The adsorption capacities of the prepared nanocomposite on the dye increased from 139.1 to 146.9 mg/g for the dye and increased from 190.3 to 196.6 mg/g for Cu (II) ions. This is attributed to the increment in the kinetic energy of the adsorbent molecules with the increment in temperature, the increased activated sites created on the PVA-co-AAm/TiO_2/SiO_2-30 nanocomposite, and the increase in kinetic motion of metal ion molecules that leads to an increase in the penetration of metal ions inside the micropores of the prepared nanocomposite as temperature increased. Also, with increasing the temperature, the speed of diffusion of dye molecules through the exterior boundary layer and in the interior holes in the nanocomposite increases with the temperature, and the amount of the adsorbed Cu (II) ions or the dye adsorption increases. The results revealed that the adsorption process is an endothermic reaction and prepared nanocomposite is a successful adsorbent for the adsorption of BB3 or Cu (II) ions from wastewater.

3.3.6 Sorption Isotherms

The sorption isotherm examines are significant in deciding the adsorption capacity of the PVA-co-AAm/TiO_2/SiO_2-30 nanocomposite to identify the character of adsorption. Langmuir, Freundlich, and Temkin isotherm models were used to fit the experimental data of the adsorption isotherm.

The Langmuir isotherm supposes that adsorption energy is a constant site and adsorption takes place on a homogeneous surface by monolayer adsorption. The Langmuir equation is expressed by Eq. (7):

$$\frac{C_e}{q_e} = \frac{1}{q_m K_L} + \frac{C_e}{q_m} \tag{7}$$

where, q_e (mg/g) is the adsorption capacity at equilibrium, q_m (mg/g) is the maximum adsorption capacity, C_e is the concentration of dye after adsorption (mg/L). K_L is the Langmuir constant; n is related to the adsorption intensity. K_L (L/g) and q_m of Langmuir isotherm obtained by plotting the curve C_e/q_e versus C_e.

Also, The favorability of PVA-co-AAm/TiO_2/SiO_2-30 nanocomposite as an adsorbent for BB3 and Cu (II) ions Langmuir adsorption constant K_L and can be represented in terms of the Langmuir isotherm is R_L which is a dimensionless separation. R_L can be calculated using Eq. (8) that describes the adsorption process whether favorable or unfavorable. R_L value is between 0–1. If $R_L > 1$ suggesting the adsorption is unfavorable, if $R_L = 1$ suggesting the adsorption is linear, if $0 < R_L < 1$ suggesting the adsorption is favorable and if R_L equals 0, it represents irreversible adsorption

$$R_L = \frac{1}{1 + K_L C_o} \tag{8}$$

The Freundlich model is an experimental equation utilized to express the multilayer adsorption on a heterogeneous surface and described by Eq. (9).

$$\ln q_e = \ln K_F + \frac{1}{n} \ln C_e \tag{9}$$

Meanwhile, K_F is Freundlich isotherm constant [(mg/g) $(L/mg)^{1/n}$] (L/g) obtained by plotting the curve *ln* q_e versus *ln* C_e and *n* is (dimensionless) the heterogeneity factor associated with the adsorption intensity and adsorption capacity.

Temkin isotherm was used to study the multi-layer adsorption and suppose that the adsorption heat of all molecules reduces linearly with the enhanced coverage of the adsorbent surface, the adsorption is described by a homogeneous distribution up to the highest binding energy. The Temkin isotherm can be illustrated by Eq. (10).

$$q_e = \frac{RT}{b_T} \ln K_T + \frac{RT}{b_T} \ln C_e, B = \frac{RT}{b_T} \tag{10}$$

where K_T is the equilibrium-binding constant ($L.mg^{-1}$) related to the maximum binding energy, B is corresponding to the adsorption heat, T is the temperature (K) and R is the universal gas constant (8.314 J/K.mol).

Figure 10(a–c) shows the experimental Langmuir, Freundlich, and Temkin isotherms plots for the removal of BB3 or Cu (II) ions solution onto PVA-co-AAm/TiO_2/SiO_2-30 nanocomposite at temperature 298°K. The resulted correlation coefficients $R^2$and the isotherm parameters (K_L, K_F, K_T, q_m, n) are scheduled in Table 3. The Langmuir model has a much closed to unity R^2 value than the other two isotherms. This corroborates the adsorption process is a monolayer onto PVA-co-AAm/TiO_2/SiO_2-30 nanocomposite. The theoretical monolayer capacities of PVA-co-AAm/TiO_2/SiO_2-30 nanocomposite ($q_{m,\,cal}$) for BB3 and Cu (II) ions were also got closer to the experimentally resulted value (Table 3).

Table 3 presents the calculated R_L values in the range of 0.0023–0.58111 and 0.377–0.936 for dye and Cu (II) ions adsorption. R_L is lower than 1 ($0 < R_L < 1$) indicates that PVA-co-AAm/TiO_2/SiO_2-30 nanocomposite is a good

Table 3 The Langmuir, Freundlich, and Temkin isotherms and correlation coefficients parameters for adsorption of BB3 and Cu (II) ions onto PVA-co-AAm/TiO_2/SiO_2-30 nanocomposites

Adsorbate	$q_{e,exp}$	Langmuir isotherm				Freundlich isotherm			Temkin isotherm		
	(mg/g)	$q_{e,cal}$ (mg/g)	K_L(L/mg)×10^{-3}	R_L	R^2	K_F (mg/g) (L/mg)$^{1/n}$	n	R^2	B (10^{-5} L/mg)	K_T	b_T L/g	$\mathbf{R^2}$
Basic blue 3	123.86	171.37	1.711	0.0023–0.5811	0.9857	56.43	2.432	0.8752	4. 11	18.27	60.28	0.8752
Cu (II) ions	190.3	226.6	1.058	0.377—0.936	0.998	122.49	4.175	0.919	4.98	17.25	60.45	0.9393

medium for the adsorption of chosen dye and Cu (II) ions. Also, the outcomes in Table 3 designate that the equilibrium results are not fitted to the Temkin or Freundlich isotherm model.

3.3.7 Sorption Kinetics

The studies of the adsorption kinetics play a critical function in estimating the optimal conditions for an adsorption process to evaluate the adsorbent features. This is because the adsorption capacity is an important parameter for determining the adsorbed amount of the pollutants (dye or metal ions) by the adsorbent. Thus, several kinetics adsorption models were modulated to assess the experimental data and to best fit the kinetics for the adsorption mechanism process of the BB3 or Cu (II) on PVA-co-AAm/TiO_2/SiO_2-30 nanocomposite. Among them (i) the pseudo-first-order model as applied in Eq. 11 (the most dependable kinetics equation appropriate merely for the quick initial phase), (ii) the pseudo-second-order model (for expecting the kinetic performance of chemical sorption as a rate-controlling advance) expressed by Eq. 12 and (iii) the intra-particle diffusion equation (supposes that the mass transfer resistance influence the binding of the contamination to the adsorbent surface) as expressed in Eq. 13.

The pseudo-first-order kinetic model is presented by Eq. (11)

$$\ln\left(q_e - q_t\right) = \ln q_{e1,cal} - K_1 t \tag{11}$$

The pseudo-second-order kinetic model is presented by Eq. (12):

$$\frac{t}{q_t} = \frac{1}{k_2 q_{e2,cal}^2} + \frac{t}{q_{e2,cal}} \tag{12}$$

q_e, $q_{e,cal}$ and q_t are the experimental, calculated, and the adsorbed amount of the dye or Cu (II) (mg/g) at time t (min), respectively. K_1 (min^{-1}) and K_2 (g/mg/min) are the pseudo-first-order and the pseudo-second-order rate constants, respectively. The linear plots of the curve *ln* (q_e—q_t) versus *time (min)* were used to calculate the values of the rate constant (K_1), meanwhile, (t/q_t) versus *time (min)* was used to calculate the values of the rate constant (K_2).

The intra-particle diffusion Eq. 13:

$$q_t = k_{id} t^{0.5} + C \tag{13}$$

where k_{id} (mg $g^{-1}min^{-0.5}$) is the intra-particle diffusion rate constant.

The experimental results fitted the kinetics models revealed above. The pseudo-first-order constants k_1, $q_{e1,cal,}$ and R^2 for the studied BB3 or Cu (II) ions adsorption onto PVA-co-AAm/TiO_2/SiO_2-30 nanocomposite are represented

Table 4 Kinetic parameters and correlation coefficients for adsorption of BB3 and Cu (II) ions onto PVA-co-AAm/TiO_2/SiO_2-30 nanocomposite

Adsorbate	$q_{e,exp}$ (mg/g)	Pseudo first order			Pseudo second order			Intra-particle diffusion model		
		K_1 (10^{-3} min^{-1})	$q_{e,cal}$ (mg/g)	R^2	K_2 (10^{-2} g. $mg^{-1}.min^{-1}$)	$q_{e,cal}$ (mg/g)	R^2	k_{ip} (mg. g^{-1}. $min^{-0.5}$)	C_i	R^2
Dye	123.9	4.975	201.01	0.9716	4.878	146.7	0.9990	7.333	40.852	0.8527
Cu (II)	190.3	7.194	233.9	0.9360	2.733	213.4	0.9986	5.213	4.649	0.9702

in Fig. 10 (d-f) and Table 4. The theoretical q_e quantity calculated from the first-order kinetic model ($q_{e1,cal}$) disagree with the practical quantity ($q_{e,exp}$), and the correlation coefficients were likewise established to be marginally lower. These outcomes represented that the pseudo-first-order kinetic model was not fitting for the adsorption of tested adsorbates.

As indicated by the results in Table 4, the values of R^2 for the pseudo-second-order kinetic model were a lot nearer to unity for the adsorbent PVA-co-AAm/TiO_2/SiO_2-30 nanocomposite. The intra-particle diffusion model represented a helpless fit to the practical data, meaning that the intra-particle diffusion was not the rate-determining step in the adsorption. The adsorption capacities determined from the pseudo-second-order model $q_{e2,cal}$ was likewise near to those obtained by experiments ($q_{e,exp}$). The pseudo-second-order model depends on the hypothesis that the rate-deciding step might be chemical sorption including valence powers via exchange or sharing of electrons between the adsorbate and the adsorbent [57]. The n and K_2 data determined from the pseudo-second-order kinetic model were higher for Cu (II) ions than BB3. Among the mentioned models, pseudo-second-order is a suitable model for fitting the adsorption process.

The adsorption capacity (q_m) of BB3 and Cu (II) ions onto PVA-co-AAm/TiO_2/SiO_2-30 nanocomposite were compared with the other adsorbents as represented in Table 5. It is apparent that PVA-co-AAm/TiO_2/SiO_2-30 nanocomposite has a good adsorption capacity comparing with other adsorbents. Consequently, the prepared nanocomposite has a good potential for the adsorption of the dyes and heavy metal ions from aqueous solutions.

3.3.8 Adsorption Thermodynamics

To describe the adsorption of BB3 and Cu (II) ions onto PVA-co-AAm/TiO_2/SiO_2-30 nanocomposite anyway the procedure is spontaneous or non-spontaneous, the thermodynamic parameters, for example, standard enthalpy change (ΔH^0), Gibbs free energy change (ΔG^0) and standard entropy change (ΔS^0) were calculated to recognize better the impact of the temperature on the adsorption process. The equilibrium constant K was used to calculate the Gibbs free energy (ΔG^0) as in Eqs. (14, 15) where R is gas constant (8.314 J/mol/K), T is the temperature in Kelvin (K),

$$\Delta G^o = \Delta H^o + \mathrm{T}\Delta S^o = -RT \ln\left(\frac{q_e}{C_e}\right) \tag{14}$$

$$\ln\left(\frac{qe}{Ce}\right) = -\frac{\Delta \mathbf{G}}{\boldsymbol{RT}} = \frac{\Delta S^o}{R} - \frac{\Delta H^o}{RT} \tag{15}$$

Additional thermodynamic parameters, such as enthalpy change (ΔH°) and entropy change (ΔS°), were calculated from Eq. (14) and illustrated in Fig. 10g:

Table 5 Comparative study between PVA-co-AAm/TiO_2/SiO_2-30 nanocomposites with other adsorbents in the literature used for wastewater treatment

Adsorbent	Adsorbate	Adsorption capacity (mg/g)	Kinetic model	Isotherm model	Refs.
Carboxymethyl-chitosan /bentonite composite	Cu (II) ions	81.4	pseudo-second order	Langmuir isotherm	[24]
Polyaniline/carboxymethyl cellulose/TiO_2 nanocomposites	Congo Red	94.28	pseudo-second order model	Langmuir isotherm	[25]
Phosphorylated polyhydroxyethyl methacrylate hydrogel	Cu (II) ions	66.3	pseudo-second order	Langmuir isotherm	[55]
hydroxyapatite/biochar nanocomposites	Cu (II) ions	99.01	pseudo-second order	Langmuir isotherm	[56]
PVA-co-AAm/TiO_2/SiO_2-30 nanocomposite	Cu (II) ions	190.3	pseudo second order	Langmuir isotherm	This study
	BB3	140.9			

Table 6 Thermodynamic parameters at different temperatures

adsorbate	Gibbs free energy ΔG^o (kJ/mol)			Enthalpy ΔH^o (kJ/mol)	Entropy ΔS^o (J/mol/K)
	298 K	308 K	318 K		
BB3	− 31.024	− 33.104	− 34.241	31.132	10.51
Cu (II) ions	− 38.013	− 40.937	− 41.985	35.965	13.11

The values of ΔH° and ΔS° were determined from (Fig. 10g) from the slope and intercept value of the linear plot of $ln\ (q_e/C_e)$ versus $1/T$. The obtained data are listed in Table 6. ΔG^0 values established here are negative for adsorption of the dye and the Cu (II) ions onto the nanocomposite. This demonstrates that the adsorption procedure is spontaneous and thermodynamically practicable. Furthermore, the ΔG^0 values decreased as the temperature increased, demonstrating an increased tendency in the degree of practicability and spontaneity of uptake of the dye or metal ions onto PVA-co-AAm/TiO_2/SiO_2-30 nanocomposite. The adsorption enthalpy change (ΔH^0) was determined to be 35.97 kJ/mol for Cu (II) ions and 31.13 kJ/mol for the BB3 adsorption onto PVA-co-AAm/TiO_2/SiO_2-30 nanocomposite, respectively. The positive values of enthalpy (ΔH^o) propose that the adsorption is chemisorption. Additionally, the positive values of ΔS^0 indicate an irregular raise of the randomness at the nanocomposite-solution interface through adsorption. In similar studies, it was reported that TiO_2 nanoparticles dispersed in chitosan grafted polyacrylamide matrix for the uptake of Sirius yellow K-CF dye from aqueous solution and the obtained results showed that the adsorption process is endothermic nature, proved the Langmuir isotherm model and compatible pseudo-second-order kinetic model [26].

3.3.9 Reuse of Adsorbents

The reuse of adsorbents after a particular procedure is perhaps the main significant properties for economic and environmental reasons. Thus, the desorption–adsorption series were carried out to examine the capability of PVA-co-AAm/TiO_2/SiO_2-30 nanocomposite for application. In this work, ethanol and sodium hydroxide (alkaline environment 0.1 M) solution were utilized as desorption medium for basic blue 3 dye. Desorption of adsorbed Cu (II) ions, was done utilizing the nitric acid solution and the reusability was assessed four times as demonstrated in Fig. 11. It was established from this figure that the adsorption of Cu (II) ions or BB3 was very little influenced. In this manner, PVA-co-AAm/TiO_2/SiO_2-30 nanocomposite can be utilized many times for water contamination remediation.

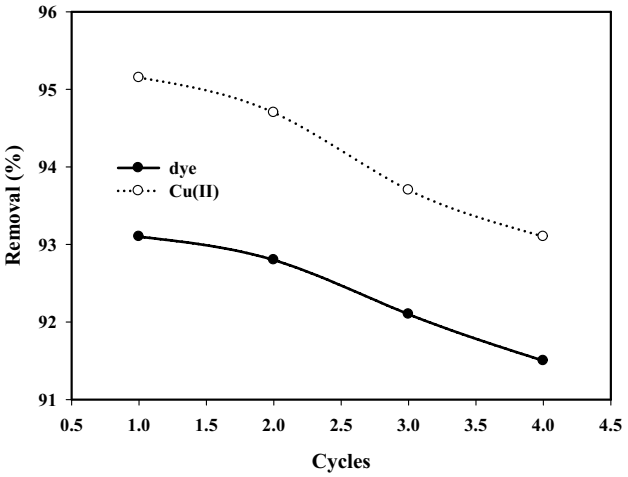

Fig. 11 Effect of cycle times on removal(%) of BB3 and Cu (II) onto PVA-co-AAm/TiO_2/SiO_2-30 nanocomposite

4 Conclusion

Novel PVA-co-AAm/TiO_2/SiO_2 nanocomposites adsorbents were synthesized by γ- by copolymerization crosslinking of PVA and AAm incorporated with TiO_2/SiO_2 nanoparticles at different irradiation doses of 10, 30, and 50 kGy for enhancement the removal and the adsorption of BB3 and Cu (II) ions and from their aqueous solutions. The effect of irradiation dose on gelation(%) and swelling(%) of PVA-co-AAm-30 copolymer and as-synthesized PVA-co-AAm/TiO_2/SiO_2 nanocomposites were studied. The gelation(%) was in the range of 90.8 to 95.7% indicating the increase in the cross-linking between PVA and AAm. The prepared PVA-co-AAm/TiO_2/SiO_2-30 had the highest swelling(%) of 197.7%. FT-IR, TEM, XRD, SEM, EDS, and DLS instruments investigated the chemical properties of PVA-co-AAm/TiO_2/SiO_2 nanocomposites. The FTIR results showed successful crosslinking between PVA backbone and AAM with the characteristic peaks of Ti–O–Ti, Si–O-Si. XRD results showed successful incorporation with the characteristic diffraction peaks of PVA-co-AAm and SiO_2 as well as TiO_2 peaks of the spinal structure of the Bragg reflections of 80% anatase and 20% rutile phases. The average crystallite size of the as-prepared nanocomposites was about 43 nm as calculated from Debeys–Scherrer equation. TEM results revealed high dispersion and uniform distribution without agglomeration of TiO_2/SiO_2 nanoparticles inside the nanocomposite with an average size of 60–70 nm. The particle size distribution of PVA-co-AAm/TiO_2/SiO_2-30 obtained from DLS was homogeneously shape with an average size of about 93.5 nm. SEM/EDS analysis confirms the detection peaks belonging to the C, O, Si, and Ti. The adsorption capacity of PVA-co-AAm-30 and as-prepared PVA-co-AAm/TiO_2/SiO_2 nanocomposites towards BB3 and Cu (II)

ions was studied. The as-prepared nanocomposites improve the adsorption capacity of dye or metal ions 3 folds compared with PVA-co-AAm-30 adsorbent. The PVA-co-AAm/TiO_2/SiO_2-30 shows the highest swelling, adsorption, and removal(%) towards BB3 and Cu (II) ions. The optimum adsorption capacity (mg/g) and removal(%) of BB3 or Cu (II) ions from their aqueous solutions onto PVA-co-AAm/TiO_2/SiO_2-30 nanocomposites were dependent on pH, temperature, initial of dye or metal concentration, and contact time. The equilibrium adsorption for BB3 was about 140.9 mg/g with the removal of 93.5% at 7 h contact time, pH 11, adsorbent dosage 0.4 g, and initial concentration 150 mg/L. While, the equilibrium adsorption for Cu (II) ions was about 190.3 mg/g with the removal of 95.2% at 6 h, pH 6, adsorbent dosage 0.4 g, and initial concentration 200 mg/L. The adsorption kinetics suggested that the adsorption of both BB3 and Cu (II) ions best agreed with the pseudo-second-order model. The adsorption isotherm illustrated that the adsorption between dye or Cu (II) ions and PVA-co-AAm/TiO_2/SiO_2 nanocomposite can be well described by Langmuir adsorption isotherms ($R^2 = 0.9857$ and 0.99). The adsorption process is endothermic and spontaneous according to thermodynamic parameters and temperature dependence data obtained using Van't Hoff plot. PVA-co-AAm/TiO_2/SiO_2 nanocomposites could be applied as an efficient and novel adsorbent for the elimination of dyes and metal cations from contaminated water with high adsorption capacity and convenient recovery.

Acknowledgements Authors would to thank National Center for Radiation Research and Technology, Egyptian Atomic Energy Authority for facilitating experiments of preparation, irradiation and apparatus used for characterization.

Author contributions AME was responsible for the conception and design, testing, data acquisition, data interpretation, writing—review, and editing. YHG was responsible for analysis and data interpretation, writing—review, and editing manuscript. All authors read, revise, and approved the final manuscript.

Funding Not applicable.

Data availability statement The data that support the findings of this study are available from the corresponding author upon reasonable request.

Declarations

Conflict of interest The authors declare that they have no competing interests and non-financial competing interests.

Consent to publish All authors approved for publication.

References

1. J.P. Vareda, A.J.M. Valente, L. Durães, Assessment of heavy metal pollution from anthropogenic activities and remediation strategies: A review. J. Environ. Manage. **246**, 101–118 (2019)
2. S.T. Akar, T. Akar, Z. Kaynak, B. Anilan, A. Cabuk, Ö. Tabak, T.A. Demir, T. Gedikbey, Removal of copper (II) ions from synthetic solution and real wastewater by the combined action of dried Trametes versicolor cells and montmorillonite. Hydrometallurgy **97**(1–2), 98–104 (2009)
3. M.K. Uddin, A review on the adsorption of heavy metals by clay minerals, with special focus on the past decade. Chem. Eng. J. **308**, 438–462 (2017)
4. M.N. Khalaf, *Green Polymers and Environmental Pollution Control* (CRC Press, Boca Raton, 2016).
5. W. Tanan, S. Saengsuwan, A one-pot microwave-assisted synthesis of IPN hydrogels based on HEMA/AM/PVA blend for enhancing Cu (II) and Pb (II) ions removal. J. Environ. Chem. Eng. **8**(2), 103469 (2020)
6. S. Zinatloo-Ajabshir, S.A. Heidari-Asil, M. Salavati-Niasari, Recyclable magnetic $ZnCo_2O_4$-based ceramic nanostructure materials fabricated by simple sonochemical route for effective sunlight-driven photocatalytic degradation of organic pollution. Ceram. Int. **47**(7), 8959–8972 (2021)
7. V. Dulman, S.-M. Cucu-Man, I. Bunia, M. Dumitras, Batch and fixed bed column studies on removal of Orange G acid dye by a weak base functionalized polymer. Desalin. Water Treat. **57**(31), 14708–14727 (2016)
8. M. Mousavi-Kamazani, S. Zinatloo-Ajabshir, M. Ghodrati, One-step sonochemical synthesis of Zn $(OH)_2$/ZnV_3O_8 nanostructures as a potent material in electrochemical hydrogen storage. J. Mater. Sci.: Mater. Electron. **31**(20), 17332–17338 (2020)
9. S. Zinatloo-Ajabshir, M. Mousavi-Kamazani, Effect of copper on improving the electrochemical storage of hydrogen in CeO_2 nanostructure fabricated by a simple and surfactant-free sonochemical pathway. Ceram. Int. **46**(17), 26548–26556 (2020)
10. S. Zinatloo-Ajabshir, M.S. Morassaei, O. Amiri, M. Salavati-Niasari, Green synthesis of dysprosium stannate nanoparticles using Ficus carica extract as photocatalyst for the degradation of organic pollutants under visible irradiation. Ceram. Int. **46**(5), 6095–6107 (2020)
11. S. Zinatloo-Ajabshir, M. Baladi, M. Salavati-Niasari, Enhanced visible-light-driven photocatalytic performance for degradation of organic contaminants using PbWO4 nanostructure fabricated by a new, simple and green sonochemical approach. Ultrason. Sonochem. **72**, 105420 (2021)
12. P. Maijan, P. Amornpitoksuk, S. Chantarak, Synthesis and characterization of poly (vinyl alcohol-g-acrylamide)/SiO2@ ZnO photocatalytic hydrogel composite for removal and degradation of methylene blue. Polymer **203**, 122771 (2020)
13. T.M. Morsi, A.M. Elbarbary, M.M. Ghobashy, S.H. Othman, Surface decontamination in fuel manufacture plants by chelating solution of nanoparticles. Radiochim. Acta **106**(5), 383–392 (2018)
14. S.H. Othman, A.M. Elbarbary, G. Rashad, T.W. Fasih, Radioiodide uptake by modified poly (glycidyl methacrylate) as anion exchange resin. Radiochim. Acta **105**(1), 75–84 (2017)
15. H.-P. Feng, L. Tang, G.-M. Zeng, Y. Zhou, Y.-C. Deng, X. Ren, B. Song, C. Liang, M.-Y. Wei, J.-F. Yu, Core-shell nanomaterials: Applications in energy storage and conversion. Adv. Coll. Interface. Sci. **267**, 26–46 (2019)
16. Y. Zhang, M. Wu, M. Wu, J. Zhu, X. Zhang, Multifunctional carbon-based nanomaterials: applications in biomolecular imaging and therapy. ACS Omega **3**(8), 9126–9145 (2018)

17. A.M. Elbarbary, I.A. Ibrahim, H.M. Shafik, S.H. Othman, Magnetic 99mTc-core-shell of polyethylene glycol/polyhydroxyethyl methacrylate based on Fe_3O_4 nanoparticles: Radiation synthesis, characterization and biodistribution study in tumor bearing mice. Adv. Powder Technol. **28**(8), 1898–1910 (2017)
18. S.H. Othman, I.A. Ibrahim, M.H. Hatab, A.M. Elbarbary, Preparation, characterization and biodistribution in quails of 99mTc-folic acid/chitosan nanostructure. Int. J. Biol. Macromol. **92**, 550–560 (2016)
19. W. Park, H. Shin, B. Choi, W.-K. Rhim, K. Na, D.K. Han, Advanced hybrid nanomaterials for biomedical applications. Prog. Mater. Sci. **114**, 100686 (2020)
20. G. Lofrano, M. Carotenuto, G. Libralato, R.F. Domingos, A. Markus, L. Dini, R.K. Gautam, D. Baldantoni, M. Rossi, S.K. Sharma, Polymer functionalized nanocomposites for metals removal from water and wastewater: an overview. Water Res. **92**, 22–37 (2016)
21. M. Ghorbani, H. Eisazadeh, Removal of COD, color, anions and heavy metals from cotton textile wastewater by using polyaniline and polypyrrole nanocomposites coated on rice husk ash. Compos. B Eng. **45**(1), 1–7 (2013)
22. S. Akbarnejad, A.A. Amooey, S. Ghasemi, High effective adsorption of acid fuchsin dye using magnetic biodegradable polymer-based nanocomposite from aqueous solutions. Microchem. J. **149**, 103966 (2019)
23. A.K. Sarkar, A. Saha, A.B. Panda, S. Pal, pH Triggered superior selective adsorption and separation of both cationic and anionic dyes and photocatalytic activity on a fully exfoliated titanate layer–natural polymer based nanocomposite. Chem. Commun. **51**(89), 16057–16060 (2015)
24. N. Gong, Y. Liu, R. Huang, Simultaneous adsorption of $Cu2^+$ and Acid fuchsin (AF) from aqueous solutions by CMC/bentonite composite. Int. J. Biol. Macromol. **115**, 580–589 (2018)
25. M. Tanzifi, M.T. Yaraki, M. Karami, S. Karimi, A.D. Kiadehi, K. Karimipour, S. Wang, Modelling of dye adsorption from aqueous solution on polyaniline/carboxymethyl cellulose/TiO_2 nanocomposites. J. Colloid Interface Sci. **519**, 154–173 (2018)
26. E. Binaeian, S.B. Zadvarzi, D. Yuan, Anionic dye uptake via composite using chitosan-polyacrylamide hydrogel as matrix containing TiO_2 nanoparticles; comprehensive adsorption studies. Int. J. Biol. Macromol. **162**, 150–162 (2020)
27. A. Awwad, M. Amer, M. Al-aqarbeh, TiO_2-kaolinite nanocomposite prepared from the Jordanian Kaolin clay: Adsorption and thermodynamics of Pb (II) and Cd (II) ions in aqueous solution, Chem. Int. (2020).
28. M. Rezakazemi, M. Sadrzadeh, T. Mohammadi, T. Matsuura, *Methods for the Preparation of Organic–Inorganic Nanocomposite Polymer Electrolyte Membranes for Fuel Cells* (Springer, Organic-Inorganic Composite Polymer Electrolyte Membranes, 2017), pp. 311–325
29. G.S. El-Sayyad, M. Abd Elkodous, A.M. El-Khawaga, M.A. Elsayed, A.I. El-Batal, M. Gobara, Merits of photocatalytic and antimicrobial applications of gamma-irradiated $Co_xNi_{1-x}Fe_2O_4/SiO_2/TiO_2$ x= 0.9 nanocomposite for pyridine removal and pathogenic bacteria/fungi disinfection implication for wastewater treatment, RSC Adv. 10(9) 5241-5259 (2020)
30. C.H. Zhu, Z.B. Hai, C.H. Cui, H.H. Li, J.F. Chen, S.H. Yu, In situ controlled synthesis of thermosensitive poly (*N*-isopropylacrylamide)/Au nanocomposite hydrogels by gamma radiation for catalytic application. Small **8**(6), 930–936 (2012)
31. A.M. Elbarbary, N.M. El-Sawy, Radiation synthesis and characterization of polyvinyl alcohol/chitosan/silver nanocomposite membranes: antimicrobial and blood compatibility studies. Polym. Bull. **74**(1), 195–212 (2017)
32. M. Micutz, R.M. Lungu, V. Circu, M. Ilis, T. Staicu, Hydrogels obtained via γ-irradiation based on poly (acrylic acid) and its copolymers with 2-hydroxyethyl methacrylate. Appl. Sci. **10**(14), 4960 (2020)
33. A.G. Chmielewski, M. Haji-Saeid, S. Ahmed, Progress in radiation processing of polymers. Nucl. Instrum. Methods Phys. Res. Sect. B **236**(1–4), 44–54 (2005)
34. E. Marin, J. Rojas, Y. Ciro, A review of polyvinyl alcohol derivatives: promising materials for pharmaceutical and biomedical applications. Afr. J. Pharm. Pharmacol **8**(24), 674–684 (2014)
35. A. Rabiee, Acrylamide-based anionic polyelectrolytes and their applications: A survey. J. Vinyl Add. Tech. **16**(2), 111–119 (2010)
36. X. Chen, A. Selloni, Introduction: titanium dioxide (TiO2) nanomaterials. Chem. Rev. **114**(19), 9281–9282 (2014)
37. M. Hdidar, S. Chouikhi, A. Fattoum, M. Arous, A. Kallel, Influence of TiO_2 rutile doping on the thermal and dielectric properties of nanocomposite films based PVA. J. Alloy. Compd. **750**, 375–383 (2018)
38. C. Anderson, A.J. Bard, An improved photocatalyst of TiO_2/SiO_2 prepared by a sol-gel synthesis. J. Phys. Chem. **99**(24), 9882–9885 (1995)
39. Y.H. Gad, A.M. Elbarbary, Radiation synthesis of Fe_3O_4/SiO_2/glycidyl methacrylate/acrylonitrile nanocomposite for adsorption of basic violet 7 dye: kinetic, isotherm, and thermodynamic study. Appl. Organomet. Chem. (2021). https://doi.org/10.1002/aoc.6258
40. N. Mahmud, A. Benamor, M.S. Nasser, M.M. Ba-Abbad, M.H. El-Naas, A.W. Mohammad, Effective heterogeneous fenton-Like degradation of malachite green dye using the core-shell Fe_3O_4@ SiO_2 nano-catalyst. ChemistrySelect **6**(4), 865–875 (2021)
41. W. Zhang, Q. Deng, Q. He, J. Song, S. Zhang, H. Wang, J. Zhou, H. Zhang, A facile synthesis of core-shell/bead-like poly (vinyl alcohol)/alginate@ PAM with good adsorption capacity, high adaptability and stability towards Cu (II)removal. Chem. Eng. J. **351**, 462–472 (2018)
42. E. Sonker, R. Tiwari, P. Adhikary, K. Kumar, S. Krishnamoorthi, Preparation of ultra-high-molecular-weight polyacrylamide by vertical solution polymerization technique. Polym. Eng. Sci. **59**(6), 1175–1181 (2019)
43. E.S. Agorku, H. Mittal, B.B. Mamba, A.C. Pandey, A.K. Mishra, Fabrication of photocatalyst based on $Eu3^+$-doped ZnS–SiO_2 and sodium alginate core shell nanocomposite. Int. J. Biol. Macromol. **70**, 143–149 (2014)
44. S. Pourjafar, A. Rahimpour, M. Jahanshahi, Synthesis and characterization of PVA/PES thin film composite nanofiltration membrane modified with TiO_2 nanoparticles for better performance and surface properties. J. Ind. Eng. Chem. **18**(4), 1398–1405 (2012)
45. M.M. Ba-Abbad, A.A.H. Kadhum, A.B. Mohamad, M.S. Takriff, K. Sopian, Synthesis and catalytic activity of TiO_2 nanoparticles for photochemical oxidation of concentrated chlorophenols under direct solar radiation. Int. J. Electrochem. Sci **7**(6), 4871–4888 (2012)
46. K. Thamaphat, P. Limsuwan, B. Ngotawornchai, Phase characterization of TiO_2 powder by XRD and TEM. Agric. Nat. Resour. **42**(5), 357–361 (2008)
47. X. Cao, J. Ma, X. Shi, Z. Ren, Effect of TiO_2 nanoparticle size on the performance of PVDF membrane. Appl. Surf. Sci. **253**(4), 2003–2010 (2006)
48. S. Zinatloo-Ajabshir, M. Salavati-Niasari, Preparation and characterization of nanocrystalline praseodymium oxide via a simple precipitation approach. J. Mater. Sci.: Mater. Electron. **26**(8), 5812–5821 (2015)
49. S. Zinatloo-Ajabshir, M. Salavati-Niasari, Synthesis of pure nanocrystalline ZrO_2 via a simple sonochemical-assisted route. J. Ind. Eng. Chem. **20**(5), 3313–3319 (2014)

50. F. Chen, J. Zhao, H. Hidaka, Highly selective deethylation of rhodamine B: adsorption and photooxidation pathways of the dye on the TiO_2/SiO_2 composite photocatalyst. Int. J. Photoenergy **5**(4), 209–217 (2003)
51. L. Zou, Y. Luo, M. Hooper, E. Hu, Removal of VOCs by photocatalysis process using adsorption enhanced TiO_2–SiO_2 catalyst. Chem. Eng. Process. **45**(11), 959–964 (2006)
52. K.A. Gebru, C. Das, Removal of Pb (II) and Cu (II) ions from wastewater using composite electrospun cellulose acetate/titanium oxide (TiO_2) adsorbent. J. Water Process Eng. **16**, 1–13 (2017)
53. S. Sakarkar, S. Muthukumaran, V. Jegatheesan, Evaluation of polyvinyl alcohol (PVA) loading in the PVA/titanium dioxide (TiO_2) thin film coating on polyvinylidene fluoride (PVDF) membrane for the removal of textile dyes. Chemosphere **257**, 127144 (2020)
54. P.M. Pakdel, S.J. Peighambardoust, Review on recent progress in chitosan-based hydrogels for wastewater treatment application. Carbohyd. Polym. **201**, 264–279 (2018)
55. A.M. Elbarbary, M.M. Ghobashy, Phosphorylation of chitosan/HEMA interpenetrating polymer network prepared by γ-radiation for metal ions removal from aqueous solutions. Carbohyd. Polym. **162**, 16–27 (2017)
56. K.-W. Jung, S.Y. Lee, J.-W. Choi, Y.J. Lee, A facile one-pot hydrothermal synthesis of hydroxyapatite/biochar nanocomposites: adsorption behavior and mechanisms for the removal of copper (II) from aqueous media. Chem. Eng. J. **369**, 529–541 (2019)
57. A. Masoumi, K. Hemmati, M. Ghaemy, Structural modification of acrylonitrile–butadiene–styrene waste as an efficient nanoadsorbent for removal of metal ions from water: isotherm, kinetic and thermodynamic study. RSC Adv. **5**(3), 1735–1744 (2015)